Seidov, D. and B. J. Haupt, Numerical study of glacial and meltwater global ocean. in *Computerized Modeling of Sedimentary Systems*, edited by Harff, J., J. Lemke and K. Stattegger, pp. 79-113, Springer, New York, 1999.

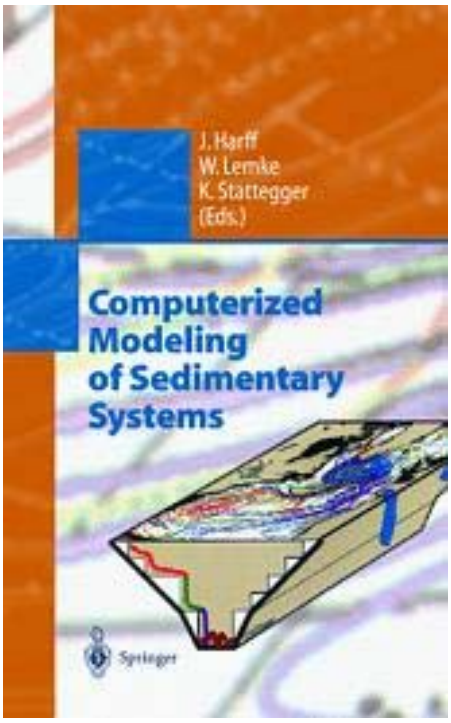

J. Harff, University of Rostock, Germany
W. Lemke, University of Rostock, Germany
K. Stattegger, University of Kiel, Germany (Eds.)

Computerized Modeling of Sedimentary Systems

Computerized modeling is a powerful tool to describe the complex interrelations between measured data and the dynamics of sedimentary systems. Complex interaction of environmental factors with natural variations and increasing anthropogenic intervention is reflected in the sedimentary record at varying scales. The understanding of these processes gives way to the reconstruction of the past and is a key to the prediction of future trends. Especially in cases where observations are limited and/or expensive, computer simulations may substitute for the lack of data. State-of-the-art research work requires a thorough knowledge of processes at the interfaces between atmosphere, hydrosphere, biosphere, and lithosphere, and is therefore an interdisciplinary approach.

Keywords: sedimentology, oceanography, mathematical geology prediction, modeling

Fields: Computer Applications in Geosciences; Math. Applications in Geosciences; Sedimentology

Written for: Graduate students and professionals engaged in the field of sedimentary basin analysis and sedimentary modeling in general

Table of Contents

Contents: From the contents: Climatic, oceanographic and biological forcing of sedimentary systems.- Trends and periodicity in the sedimentary record as a response to environmental changes.- Space-time models of the basin fill.

1998 . Approx. 480 pp. 212 figs. 57 in color, 37 tabs.
ISBN 3-540-64109-2
Hardcover
DM 198,- /US$ 129,-
Publication date: October, 1998

Book category: Proceedings
Publication language English

Seidov, D. and B. J. Haupt, Numerical study of glacial and meltwater global ocean. in *Computerized Modeling of Sedimentary Systems*, edited by Harff, J., J. Lemke and K. Stattegger, pp. 79-113, Springer, New York, 1999.

NUMERICAL STUDY OF GLACIAL AND MELTWATER GLOBAL OCEAN THERMOHALINE CONVEYOR

Dan Seidov
Geologisch–Paläontologisches Institut, Universität Kiel, Kiel, Germany, now at: Earth System Science Center, Pennsylvania State University, University Park, USA

Bernd J. Haupt
Sonderforschungsbereich 313, Universität Kiel, Kiel, Germany

Abstract

Circulation regimes of the World Ocean and the North Atlantic at present, at the last glacial maximum, and at a subsequent meltwater event (MWE) are simulated using a combination of a global ocean circulation model, a sediment transport model (in the North Atlantic) and a semi–lagrangian trajectory tracing model (for both the World Ocean and the North Atlantic). The sedimentation model reveals differences in sediment deposition in the North Atlantic linked to past and present circulation regimes. The trajectory tracing model helps to visualize the true three–dimensional water transport which is not accessed by traditional ocean circulation modeling. Our simulations indicate that although the glacial mode of the conveyor was operationally different and substantially weaker as compared to the present day mode, the major changes of the deep global ocean conveyor occurred only at the MWE. Globally, these changes led to reversal of the Indian–Atlantic branch of the deep conveyor due to a complete cessation of North Atlantic Deep Water production. This complete termination of NADW production was caused by a very localized meltwater impact which led to a suppression of the deep convection in the key convection sites. In the North Atlantic a reverse conveyor took over the entire middle and high latitudes causing water transport and sedimentation very different from the present–day regime.

Introduction

The ocean thermohaline circulation is often referred to as a global ‘conveyor’ [Gordon, 1986; Broecker and Denton, 1989; Broecker, 1991; a review in Gordon et al., 1992]. It is common knowledge that the global ocean thermohaline circulation is strongly controlled by the production of the North Atlantic Deep Water (NADW). Warm and salty subtropical water is carried to the high latitudes in the North Atlantic (NA) by the North Atlantic Current. It is cooled there and descends to set forth the deep ocean current system which is believed to be a global feature, a conveyor. Since the conveyor is mainly driven by latitudinal density gradients, which in high latitudes are controlled primarily by salinity, the density–driven conveyor is also referred to as the global ‘salinity conveyor belt’ [Broecker, 1991]. The intriguing part of the problem is that the driving mechanism of change is thought to be very localized, with the key area of convection in the northern NA being surprisingly small with respect to the global ocean volume.

Both high–latitudinal salinity and temperature varied dramatically during the last several hundred years during the major glacial–interglacial cycles, and many believe that the global thermohaline ocean circulation was radically different at various stages during the Late Quaternary. A strong positive feedback between a curtailed conveyor and ongoing glaciation or deglaciation may be expected. As sediment is transported by ocean currents, the conveyor history is thought to be imprinted in the seabed sediment. Hence, the ocean past circulation can be reconstructed, in principle, on the basis of sediment accumulation records [Einsele, 1992; Hsü, 1989]. Alternatively, one can try to reconstruct sediment transport using simulated past ocean circulation. Finally, the two approaches may be tied together by a Lagrangian approach to compare sediment transport and water volume motion. The results of such a multi–thread approach to past ocean climatology can help both sedimentologists and oceanographers to predict future change of the sediment transport and ocean climate on the basis of top–analogues given by past circulation patterns.

This paper reviews some of our recent paleoceanographic modeling and presents some of our new results on the modeling of the global and North Atlantic paleocirculation and sedimentation regimes. The emphasis is on sedimentation and water motion inferred using two specially designed models; a three–dimensional (3–D) sediment transport model and a semi–Lagrangian water transport model which are used as add–ons to traditional ocean general circulation models (OGCMs).

In the following sections we give an overview of the setup of past ocean sea surface boundary conditions, a brief description of the employed numerical models, a short review of the results of our recent regional modeling of the NA

circulation and sedimentation, and a display of some global conveyor simulations at two time slices, these being at and after the last glacial maximum.

Time Slices and Data

The global, and even regional basin–scale numerical modeling of ocean circulation necessitates a regular–grid coverage of the sea surface with hydrological data comprising sea surface boundary conditions – a requirement not easily met in paleoceanographic modeling. In fact only the glacial–to–interglacial cycle of the last 20 000 years has the sea surface data coverage that might be seriously considered as suitable for ocean circulation simulations based on proxy data. Moreover, only the last glacial maximum (LGM) has a global sea surface temperature (SST) array compiled by CLIMAP [1981]. This data set has recently received much criticism because it is thought that the tropics are to warm [Guilderson et al., 1994; Beck et al., 1997; Webb et al., 1997]. However, this data set remains the only global SST compilation currently available.

Thermohaline circulation cannot be properly modeled without knowing salinity distribution. Hence, sea surface salinity (or equivalent freshwater fluxes across the sea surface needed to maintain the observed salinity), should be known along with the SST to provide complete thermohaline sea surface boundary conditions for computing ocean circulation. Moreover, freshwater discharges in the high latitudes of the North Atlantic may have enough power to profound by affect the circulation in this basin and perhaps worldwide. The freshwater fluxes are therefore thought to be a major cause of past ocean climate changes linked to the global salinity conveyor belt operation.

There was a substantial increase of salinity of the World Ocean at the LGM due to large amount of freshwater deposited in the continental and shelf ice sheets. Some authors assume values as high as 1 psu [Duplessy et al., 1988; Fichefet et al., 1994]. The removal of the freshwater stored in the ice sheets may be considered as more or less a global feature over large areas because freshwater was mainly evaporated from the ocean. Therefore the glacial increase of sea surface salinity (SSS) may be assumed, although to the first approximation only, as a uniform increase. On the contrary, the deglacial freshwater discharges were tied to high latitudes, mostly in the North Atlantic and perhaps also in the Southern Ocean (as there are many indications of an interhemispheric synchrony of deglaciations (e.g., Bard et al., 1997), and therefore cannot be inserted into a model as a homogeneous salinity decrease everywhere. Furthermore, the distribution and intensity of such freshwater fluxes may become the most important paleoceanographic information in computerized studies of ancient ocean conveyors. In essence, the high–latitude SSS data become the major unknown and their absence would jeopardize any systematic use of an OGCM in ocean paleoclimate studies.

The situation is not as hopeless however. The conveyor operation is thought to be hampered by suppression of the deep convection in the northern NA and in the Nordic Seas because of major meltwater discharges. Fortunately, these areas are relatively well covered by proxy data and corresponding paleoreconstructions which provide both SST and SSS for LGM and a subsequent meltwater event near 13 000 ^{14}C years here abbreviated as MWE. Based on these proxies for the LGM and MWE time slices, SST and SSS to the north of 40°N were reconstructed [Duplessy et al., 1988; Sarnthein et al., 1995]. These reconstructions provided a basis for setting up thermohaline sea surface conditions on a 1°x1° regular grid in the entire NA north of 10°N [Seidov et al., 1996]. Such boundary conditions were compiled for both LGM and MWE. Seidov et al. [1996] used these data in their simulations of the NA circulation during these two time slices. To compare the emerging circulation patterns to the present day circulation, a control (modern) run was also carried out. In the control run modern sea surface climatology from Levitus [1982] was used. The control run is henceforth referred to as the Holocene/Modern (HM) experiment.

To simulate the ocean circulation one needs not only the thermohaline sea surface forcing, but the wind stress data as well. The wind stresses for LGM and for the control run were extracted from the output of the Hamburg atmosphere general circulation model [Lautenschlager and Herterich, 1991; Lorenz et al., 1996]. At LGM this model is driven by the CLIMAP [1981] SST, whereas the modern run was driven by present–day sea surface climatology. The MWE wind was assumed to be the same as at LGM.

Thermohaline sea surface conditions and the wind stress distributions comprise the necessary boundary conditions allowing simulation of the past ocean annual mean circulation. Table 1 gives the sources of the data used to compile the regional NA regular arrays of boundary conditions.

Based on these regional NA data, global distributions of SST from CLIMAP [1981] were updated in the northern NA and the Nordic Seas to form LGM and MWE SST distributions. Present day sea surface salinity was increased everywhere by 0.8 psu (to compromise between the upper limit estimate of 1 psu and smooth connection of the low and high latitudes in the NA; see [Seidov et al., 1996]) and the regional NA LGM SSS replaced the modified SSS to the north of 40°N to form the global LGM and MWE SSS distribution. Modern mean annual SST and SSS are specified from new ocean climatological data sets [Levitus and Boyer, 1994; Levitus et al., 1994], except for the area south of Greenland where some additional cooling of up to 2°C mimicking cold spells from Greenland was needed to obtain present day annual NADW production.

Numerical Models

The core of our approach is a combination of the traditional, albeit rather coarse, resolution simulations of the global ocean circulation and the NA circulation with somewhat better resolution using an OGCM together with a new technique

of tracing the water volume transport based on the output from the OGCM. This approach was first suggested in Seidov and Haupt [1997] in regional NA modeling and then was applied to past global conveyor simulations. An analogous approach has been advanced recently by Drijfhout et al. [1996], who traced the present day conveyor. Another new feature is sediment transport modeling which takes into account the major conveyor control, that is the deep ocean convection.

OGCM. Two different numerical models of the general ocean circulation were used in the regional NA and global conveyor studies. For the regional NA studies we employed a planetary geostrophic ocean circulation model especially designed for coarse–resolution, large–scale ocean circulation studies. The basics of this model are described in Seidov [1996] and Seidov and Prien [1996]. The model uses the fact that the momentum balance away from the equator is predominantly geostrophic, and therefore it belongs to the "intermediate" or "planetary geostrophic" class of models [Hasselmann, 1982; Seidov, 1986, 1996; Colin de Verdière , 1988; Maier–Reimer et al., 1991, 1993; Zhang et al., 1992]. Except for the linear dynamics inherent to planetary geostrophic models, such models retain all features of the most advanced primitive equation models (PEM) that are the present–day standards in physical oceanography [e.g., Bryan, 1969, Cox, 1984, Semtner, 1986]. Planetary geostrophic formalism allows some simplifications of the momentum and vorticity balance equations, and a longer time step, and consequently becomes computationally more effective. Parallel runs have been made on a coarse–resolution grid using this model and the Geophysical Fluid Dynamics Laboratory (GFDL) [Bryan, 1969; Cox, 1984; Pacanowski et al., 1993], a PEM. Seidov and Prien [1996] have shown that results of this planetary geostrophic model match well with the performance of the GFDL model. However, since the planetary–geostrophic approach may lead to significant discrepancies in the equatorial region, the global ocean circulation was simulated using the GFDL–Modular Ocean Model (MOM, version 1.1) (Cox, 1984; Pacanowski et al., 1993).

Any OGCM contains a procedure to allow convective mixing that develops due to hydrostatic instability if denser water is formed (or advected) over lighter water. This is the key process for deep water production and transport. As done commonly in an OGCM, this instability is accommodated by mixing water vertically until it regains complete hydrostatic stability [Cox, 1984]. This vertical adjustment takes place as a step process with several successive mixings of adjacent layers until complete hydrostatic stability is restored. As the water convects, the particles associated with the mixing volumes exchange their positions vertically, and hence the convection facilitates deep ventilation.

Ocean sedimentation model. The sedimentation model employed here was designed by Haupt [1995] and tested in Haupt et al. [1994, 1995]. It is a large–scale sedimentation model consisting of two components: (1) a 3–D sediment transport model in the ocean interior, and (2) a 2–D sediment transport model in a thin near–bottom layer following smoothed bottom topography. The 3–D component models the advection–diffusion of sediment similar to the equations of advection–diffusion of heat and salt in the OGCM, and includes an added term to compute the settling of sediment in the water column.

The 3–D component of the sedimentation model simulates the lateral transport and the entry of sediment particles at the sea surface, including the entry of ice–rafted sedimentary material. The supply of large–grain sediment at the sea surface can be increased or decreased depending on the amount of icebergs injected into the open ocean due to decay of major ice sheets. The icebergs distribution over the NA in the past can be inferred from analyses of proxy data from foraminifera [e.g. Maslin et al, 1995]. The mass of sediment covering the sea floor depends only on the balance of sources and sinks, whereas the spatial variation of sedimentation rates depends on the circulation pattern and particle grain size. The 2–D model is initialized at every time step by the exchange of sediment between the ocean body and the ocean floor. The sediment in the bottom layer is transported by a corrected benthic flow which is largely a projection of the OGCM velocity field onto the smoothed bottom layer (1 cm thick). Additionally, the near–bottom velocities are reduced to take bottom friction into account [Miller et al., 1977; Zanke, 1978; Sündermann, 1983].

The impact of convection was not included in the previous version of the sedimentation model [Haupt et al., 1994]. In the updated version the convection is incorporated in the form of convection depths from the OGCM (Seidov and Haupt, 1997). Vertical mixing, similar to that employed in the OGCM, is applied to concentration. The sediment transport model 'knows' when to mix water because we have encoded the convection depths in the velocity field as an additional parameter. When used in the sedimentation model, this information is decoded to enable vertical mixing in the grid points where convection occurs (see below in the discussion of convection patterns).

Particle–tracing model. The water volume trajectory–tracing model was developed by Haupt [1995] and was employed to trace particle drifts in the northern North Atlantic [Haupt et al., 1994, 1995]. This model exercises a hybrid Eulerian–Lagrangian (or semi–Lagrangian) approach; the velocity components are interpolated to the current positions of the Lagrangian particles from the nearby grid points of a Eulerian numerical grid. As in the sediment transport model described above, the Eulerian velocity field is provided by the OGCM, whereas the coordinates of Lagrangian particles are calculated straightforwardly, using the Lagrangian velocity along the trajectory.

As we have emphasized above, ventilating convection induced by hydrostatic instability is included in all three components of our simulations. The semi–Lagrangian trajectory–tracing model of Haupt et al. [1994] was upgraded in Seidov and Haupt [1997] to facilitate vertical ventilation in convective 'chimneys' (Send and Marshall [1995] show that ventilating convection occurs as water mixing in water columns or 'chimneys'). Here the velocity field from the OGCM is

supplemented by the convection depths showing where and to what depth the vertically mixing volume should be propelled in the turbulent chimney. The detail discussion of the parameterization of chimney mixing in the particle–tracing model is given in Seidov and Haupt [1997].

More details of the sediment transport model and the particle–tracing model can be also found in Haupt et al. [1997; see this volume].

The Setup of Numerical Experiments

The numerical experiments in both the regional NA and the global circulation cases have been carried out in two steps. First, the OGCM has been run using the appropriate boundary conditions. Integration in time was continued for several thousand years in the regional and extended over 10,000 years in the global runs to gain absolutely stationary solutions. The for both modern and LGM conditions, the steady state current velocities were used to calculate the trajectories of the particles that move with the water volumes. The MWE velocity field is the result of integration over only 500 years from the LGM steady state with the LGM sea surface conditions replaced by the MWE ones (the duration of this meltwater event is estimated to be of several hundreds to a thousand years [Sarnthein et al., 1995]).

The regional NA study includes modeling of sediment transport, that is, these simulations comprise a threefold approach. The global ocean circulation modeling at this stage employs only the OGCM and trajectory tracing models, and therefore forms a twofold approach to water transport and ventilation problem.

For the regional NA studies we used a 2°x2° grid with 12 vertical levels. In view of uncertainties of the past sea surface conditions, and in order to facilitate multiple runs extended over 10 years with different parameter settings, employed a coarse resolution of 6°x4° in longitude and latitude respectively with 12 vertical levels. Although all major currents, except for the largely wind–driven Antarctic Circumpolar Current (ACC), are 2–3 times weaker than the observed ones, most of these currents are still clearly seen on the vector maps. At the same time, the meridional thermohaline overturning, which largely depends on the deep convection and isopycnal outcrop, is modeled far better than the horizontal flows. For the present day overturning we have obtained a value that agrees well with experiments of much finer resolution. The overturning in the NA, which comprises the NADW production, amounts to 23 Sv (1 Sv=10^6 m^3/s), for comparison Antarctic Bottom Water (AABW) inflow into the Atlantic Ocean is about 9 Sv. Since we are mainly interested in the major changes in conveyor operation and rely only on the relative changes of the conveyor intensity, the coarse resolution is legitimate for global paleocirculation studies such as that presented here. We therefore consider it to be sufficient for the semi–lagrangian simulations which are the core of our investigation.

In contrast to sensitivity studies which operate with so–called mixed boundary conditions (e.g., Manabe and Stouffer, 1994; Rahmstorf, 1995), we restore the upper layer thermohaline fields to the specified sea surface temperature (SST) and sea surface salinity (SSS). The sea surface boundary conditions are described the in previous section. In our study, the important reason for the chosen approach is the local nature of the freshwater driving. Indeed, the LGM sea surface condition were disturbed by the meltwater invasion only in the small area in the northern NA and Norwegian–Greenland Seas where the reliable the proxy data are available (see above). This restoring technique implies that the freshwater fluxes were those to maintain the reconstructed SSS in these areas. In fact we just diagnose the circulation regimes which would satisfy the 'observed' sea surface conditions.

North Atlantic Sediment Transport and Water Motion

OGCM Results. Here we briefly review our regional NA modeling. More details can be found in Seidov et al. [1996] and Seidov and Haupt [1997]. The meridional overturning streamfunction (Figure 1) which gives the general impression of the overall thermohaline meridional circulation, conforms to a simple scheme that has emerged from numerous computer simulations of differing complexity [e.g., England, 1993; Toggweiler et al., 1989; Maier–Reimer et al., 1991; Wright and Stocker, 1991; Fichefet et al., 1994; Rahmstorf, 1994; Sakai and Peltier, 1995; Manabe and Stouffer, 1995]. Today's forward or clockwise (as seen from the eastern boundary looking west through a vertical plane) gyre of the salinity conveyor occupies most of the ocean from the surface–subsurface layers to a depth of 3 km. This gyre conveys NADW and is thought of as the main wheel of the modern ocean climate. A much weaker abyssal reverse (counterclockwise) gyre conveys AABW (largely in the deepest layer, i.e., below 3 km). Its return (southward) flow joins the southward flow of NADW between 3 and 4 km. In addition, there is a weak, shallow, wind–driven reverse (counterclockwise) gyre in the mid to high latitudes, induced by Ekman convergence in the subtropics.

Note that although glacial NADW production is 8 Sv, much lower than today's value of 13 Sv, the intensity of the glacial conveyor is comparable to that of modern times. If we quantify the southward transport at 30°N, the Upper NADW outflow, or forward conveyor branch, does indeed rise to only 8 Sv (also see the inventory of the glacial water masses given by, e.g., Oppo and Lehman [1993] and Oppo et al. [1995]). However, if we take into account the deep reverse branch comprising AABW and its mixture with lower NADW still produced in the central northern Atlantic (see below in the discussion of convection patterns), the total transport amounts to 12 Sv, which gives almost the same intensity of the deep water outflow as the present–day North Atlantic combined deep outflow. The intensity of this NADW–depleted conveyor, similar to present–day conveyors' intensity, seems to fit well the recent finding based on proxy data analysis [Yu et al., 1996]. However, the modern overturning strength is too low. A slight cooling of the sea surface to the southeast

of Greenland and in the Nordic Seas may easily double the NADW production (see the next section). This is because the sea surface density taken as averages of summer and winter values is somewhat biased toward summer values, and therefore the convection is not deep enough to form the vigorous observed present–day overturning. Yet we may consider the numbers as a first approximation, keeping in mind that the glacial conveyor was probably relatively even weaker than our regional modeling indicates. Hence, we believe that the glacial conveyor was probably still noticeably weaker than the modern one, in contrast to what is suggested by Yu et al. [1996]. The global circulation modeling with sea surface cooled down by 2°C to the east of Greenland between 60° and 65°N gave 22 Sv NADW production (see below), which is probably too high; if one mediates the regional and global results there would be about 18 Sv, a number most appropriate for a coarse resolution study. This would give a twice weaker LGM forward conveyor but still comparable outflow which would fit the idea of still intensive glacial thermohaline circulation [Yu et al., 1996; Webb et al., 1997].

As we have already noted, the 3–D conveyor is essentially more complex than its 2–D image given by the total meridional overturning. The velocity fields are discussed in great detail in Seidov et al. [1996] and Seidov and Haupt [1997]. Here we briefly overview how the glacial and MWE currents differ from the modern ones. The present–day, LGM, and MWE simulated velocity fields may be inspected in Seidov et al. (1996). The most noticeable feature is the deviation of the paleo–North Atlantic Drift from its modern northeastern path. Strong zonality of the subpolar front indicates a reduced supply of water that can be downwelled as NADW in the northern North Atlantic and the NGS. Moreover, the route of the return southward flow in the deep ocean changed radically, a robust feature emerging in all our glacial experiments regardless of complexity. In the eastern part of the basin, the incursion of AABW dominates the near–bed transport up to the Faeroe–Shetland Ridge, in agreement with the water mass contouring by Sarnthein et al. [1994]. The most striking feature of the MWE currents in addition to the changes found at LGM is the reversal of the Norwegian Current and the inflow–outflow regime in the Norwegian–Greenland Seas (see Seidov et al. [1996] for details). Hence the redeposited sediment in the eastern mid to high latitudes might be of different origin. Today, sediment drifts there transport material largely from northeast to west and southwest. In contrast, during the LGM some sediment drifts could change direction of transport to redeposit the grains from south to north and northwest.

Today's southward deep return current is a deep ocean western boundary flow forming a strong countercurrent under the Gulf Stream. This western boundary current is well recognized as the most prominent feature of the thermohaline circulation [Stommel and Arons, 1960]. Though a noticeably weaker western boundary current still existed at the LGM and MWE, the descending branch returned to the southwestern basin largely as a broad zonal westward flow in the mid latitudes. The glacial countercurrent under the paleo–Gulf Stream was weaker, deeper, and farther eastward. At the LGM a southward deep ocean flow originated near the Rockall Plateau at depth of about 2 km, occurring in the eastern part of the basin, rather than in the western part as today. This particular feature of the computer model in the eastern North Atlantic is again in good agreement with the contouring by Sarnthein et al. [1994]. Using the trajectory–tracing model below, we demonstrate that the simulated glacial deep water indeed moved along the eastern flank of the Mid–Atlantic Ridge. Therefore as water in the western deep Atlantic contained more AABW at the LGM, the deep and abyssal water during the glacial time was older than at present.

To understand the mechanism of change of deep water formation, one should consider changes in the convection regime. The modern deep convection sites are found mainly in the NGS, east and south of Iceland, and in the Labrador Sea. The present–day convection pattern in our calculations is consistent with the patterns given by Maier–Reimer et al. [1993], Toggweiler et al. [1989], and Rahmstorf [1995]. Shallow convection starts in the Gulf Stream area and marks a further progression of subtropical water to high latitudes carried by the North Atlantic Current becoming deeper as it progresses northeastward and westward around the Greenland coast.

The major feature of glacial convection, as compared to its modern state, was the far weaker glacial convection in the NGS and the southward shift of the main convection sites. The maximum ventilation at the LGM occurred in the mid–North Atlantic between 50° and 60°N. This result is well supported by proxy data [Duplessy et al., 1988; Sarnthein et al., 1995]. A southward shift of both the convection sites and the polar front led to a decrease in the northward transport of warm and salty water. Hence a positive feedback worked to establish the glacial mode of circulation. An even farther southward shift of the convection was limited by Ekman pumping in the subtropics which protected the major anticyclonic gyre from shrinking even more, i.e., providing a negative feedback to balance the positive one. The MWE convection sites were shifted further southward and the convection was very shallow, penetrating no deeper than 600 m in the central North Atlantic. There was no convection to the north of 50°N and the Nordic Seas were completely convection–free during that time slice [Seidov et al., 1996].

Sediment accumulation rates and sediment transport. Total sediment accumulation is governed by the requirement that sources and sinks balance at the sea surface and be the same for all three time slices. The spatial distribution of sediment is however different, and reveals two distinctly different circulation modes between present, and at the LGM and MWE. Figure 2 presents the sediment rates for the three chosen time slices. A very high accumulation rate associated with the Holocene/Modern mode of circulation is found in the vicinity of Iceland in the Irminger Basin, along the Reykjanes Ridge at both the south and north sides of Iceland, at the Rockall Plateau, and in the NGS (Figure 2a). This is in agreement

with the present–day concept of sediment trapping in these areas [McCave and Tucholke, 1986; Bohrmann et al., 1990; Wold, 1992]. We find that the modeled sediment accumulation rates are smaller than those which have been measured. This is because of the low eolian sediment input and also because of the missing lateral input [Haupt, 1995]. The sediment is transported by the deep western southward boundary current with local maxima near Newfoundland and farther to the south in and near the Caribbean [McCave and Tucholke, 1986]. We note that Iceland and the Caribbean are represented by seamounts in the model bottom topography; hence the nonzero accumulation rates are artifacts at the exact positions of these islands.

As the glacial North Atlantic Current diverged from today's northeastern path, the accumulation rate in the Iceland and Irminger Basins dropped, and most of the sediment mass was spread over the abyssal valley in the Canary Basin (Figure 2b). Note that although the sedimentation rate is far lower there than in the Iceland Basin, the sediment mass is roughly the same because bottom area in the latitude–longitude grid cells increases rapidly to the south. A relatively high glacial accumulation rate is found in the Newfoundland Basin. However, we do not see continuous southward sediment transport along the American coast, a signature of all our experiments based on the modern ocean surface climatology. Instead, a noticeable southward sediment transport is found at the eastern flank of the Mid–Atlantic Ridge.

Though an increased northward incursion of AABW at the LGM in the eastern North Atlantic is consistent with the contouring by Sarnthein et al. [1994], the conclusions about an increased reverse abyssal gyre cannot be attributed likewise to the western part of the basin. Indeed, the southward transport, though noticeably curtailed, still existed in the western deep ocean. Analysis of the velocity maps suggests (and trajectory analysis confirms; see below) that in the west the northward flow of AABW at LGM was probably the same as or weaker than today's. Simultaneously, the eastern flank of the glacial AABW intrusion (initially through the Vema Fracture Zone) was enhanced considerably. The exchange between the eastern and northern parts of the deep North Atlantic was stronger at the LGM than today.

As the meltwater North Atlantic Current diverged from today's northeastern path, the accumulation rate in the Iceland and Irminger Basins dropped and a significant part of the sediment mass was spread over the abyssal valley in the Canary Basin (Figure 2c). Note that although the sedimentation rate is far lower there than in the Iceland Basin, the sediment mass is roughly the same because bottom area in the latitude/longitude grid cells increases rapidly to the south. The sedimentation rate around Iceland decreased by over a factor of two as compared with its modern value (compare Figure 2a and 2b). This is mainly because of the absence of ventilating convection both in the NGS and in the Irminger Sea. At the LGM, a relatively high glacial accumulation rate still emerges in the model in the Newfoundland Basin (Figure 2b). However, we do not see continuous southward sediment transport along the North American coast, a signature of all our experiments based on the modern ocean surface climatology. Instead, a noticeable southward sediment transport is found at the eastern flank of the Mid–Atlantic Ridge. At the MWE this tendency is increased significantly. The accumulation rate in the Newfoundland Basin decreased in comparison with the LGM run, whereas deposition was stronger at the eastern flank of the Mid–Atlantic Ridge. The area between Newfoundland and the Caribbean is almost totally free of sediment deposition.

Trajectory tracing. Although most of the features common to the three sediment transport patterns (the HM, LGM and MWE) can be explained by comparing them with the circulation patterns, fundamental differences between glacial and interglacial ventilation and sedimentation regimes cannot be revealed using solely the velocity maps. The transport in a transit area of intense ventilation can differ principally depending on whether convection is taken into account or ignored. Let us hypothesize that a velocity field is not computed using a prognostic circulation model, but is instead diagnostically calculated from the ocean climatology, e.g., using Levitus [1982] data. These climatological fields were formed by all processes including convection. However, the convection is not present in the data directly. Moreover, the convection pattern cannot be reconstructed using these data without running a prognostic model. Hence direct impact of convection on the water motion is missed from diagnostic calculations based on these climatological data. In other words, diagnostic velocity would contain no information about convection because hydrostatic instability was removed from the processed climatological data. This means that the Lagrangian particles whose trajectories were calculated on the basis of the observed ocean climatology instead of a prognostic model would drift along the trajectories undisturbed by convection, and therefore these simulated trajectories would be wrong.

In our experiments, the particles illustrating the flow were deployed in different areas in the northern NA (Figure 3 in Seidov and Haupt, 1997). In each of the areas, about 30 particles started to travel through the Eulerian velocity fields in all three cases — the HM, MWE and LGM. In the following maps (Figure 3 and Figure 4) we employ two different techniques to show the trajectories. In Figure 3 the trajectories are colored to show the depth of a particle. (convection sites are depicted by different shades of gray: the deeper the convection, the darker the shade). We use the sunlight spectrum colors, from dark red in the uppermost layer (< 100 m) to violet and black in the two deepest layers, to visualize vertical migration of the water parcels. In contrast, Figure 4 shows the particles' pathways with both depth and elapsed time shown in small rectangles attached to the trajectories (only two pairs of the trajectories are repeated in the black and white Figure 4). Although the model time in the trajectory–tracing calculations was over 500 years, only the tracks for the first 100–200 years of the elapsed time are shown in the maps to avoid confusion.

A striking feature of the trajectory map is the change in the glacial deep ocean circulation regime which is not so obvious from the velocity maps. This change is far more complex than a simple increase in the zonality of the surface current, a well–known feature of the LGM surface circulation [CLIMAP, 1981; Ruddiman and McIntyre, 1981; Kellogg, 1980].

The deep water production at the LGM is found in the model only in the central part of the north central North Atlantic (Figure 3), which is in agreement with the convection pattern in Figure 4b. We note that water descends in the subpolar gyre in spite of upward motion induced by Ekman divergence. Hence thermohaline currents would drive water along isopycnals in the subsurface layers regardless of ventilating convection; i.e., ventilation of subsurface and intermediate water would occur regardless of deep convection. The pronounced convective chimney forms an intensive cyclonic circulation around a homogenized column of high–density water (Figure 3b). As particles deployed at the surface during the LGM became trapped inside this column, they were propelled downward, forming most of the 8 Sv of glacial NADW (see above).

Figure 3b indicates that there was some cold intermediate water produced in the NGS at the LGM. This water, flowing farther into the North Atlantic over the Greenland–Iceland sill, was not dense enough to subduct under the intermediate to deep water formed in the central part of the subpolar gyre. It mixed with the subpolar water and stayed at an intermediate depth flowing along the S–shaped route at that depth in the north central part of the basin (see in Plates 1d and 2b in Seidov and Haupt, 1997). Most of the deep return flow occurred along the eastern slope of the Mid–Atlantic Ridge, though some water still contoured the American east coast. In contrast, water sinking in the NGS today is dense enough to descend even deeper after spilling over the sills into the North Atlantic. Together with the portion of NADW formed east of Greenland and in the Labrador Sea, this water travels southward in the western boundary current comprising most of the 13 Sv of simulated modern NADW outflow. Most of the present–day deep flow contours the American east coast, and a smaller portion is routed along the west slope of the Mid–Atlantic Ridge. We point out that the curtailment of the forward conveyor in the western part of the ocean was not complete. This implies that the conclusions based on analysis of the glacial proxy data assembled along the eastern meridional sections probably are not valid for the western part of the basin.

Figure 3a and 3b compare present and the glacial trajectories' 'spaghetti' in the subtropical anticyclonic gyre. The modern and LGM trajectory maps conform to the Luyten–Pedlosky–Stommel (LPS) ventilated thermocline theory [Luyten et al., 1983] and the computer experiment of Cox and Bryan [1984]. The thermocline in the subtropics is maintained by Ekman pumping. Therefore as water circulates in the gyre, it descends and ventilates the thermocline. The water is brought up to subsurface layers in the western boundary along upward sloping isopycnals (orange–colored segments of the trajectories in the vicinity of the western boundary in Figure 3). Flowing eastward, in the segment of western boundary current outflow, the water convects because of heat loss to the atmosphere (because the specified SST is colder than the outflowing subsurface water in this outflow zone). This shallow convection is shown in light gray in Figure 3. The subsurface water parcels in this ventilation zone come in contact with the atmosphere. They then start to descend again to repeat the whole ventilation cycle. Those water parcels which flow northeastward below the convection depth do not contact the atmosphere again and therefore do not ventilate. Yet, at any given time, new water parcels descend from the surface in the ventilation zone. However, ventilation is restricted to the central and western parts of the gyre. In complete agreement with the LPS theory, there is a shadow zone attached to the eastern boundary, practically unreachable for ventilation. Modern elapsed times (Figure 3a) for a single ventilation cycle in the gyre agree well with the estimates of Cox and Bryan [1984]; short loops have an advection age of no more than 3 to 5 years before the water returns to the ventilation zone, whereas the longer paths in the subtropical gyre take more than 10 to 15 years to return to ventilation zone. It is obvious from the colors of the trajectories in Figure 3 that the glacial thermocline is far deeper ventilated than its modern analogue. There is evidence [Slowey and Curry, 1992, 1995] that the subtropical thermocline was indeed better ventilated during the last glacial period. As Figure 4 reveals, our Lagrangian calculations agree well with these findings.

Figures 3 and 4 indicate that the speed of the particles in the upper and intermediate layers was not lower at the LGM than today. The deep and abyssal glacial flows, though routed differently from today, were even stronger in the eastern part of the basin. This confirms the concept that the LGM conveyor was at least as intense as the present one [Yu et al., 1996; Boyle, 1996]. However we stress that, in contrast to a similar or even higher intensity meridional conveyor at intermediate depths, the forward conveyor was definitely weaker at the upper to intermediate depths.

The MWE trajectories indicate that at that time slice there was no ventilation of the deep ocean in the NA (Figure 3c), although there was still quite intensive ventilation of the subtropical thermocline. The spaghetti form of the MWE trajectories indicate also that the Nordic Seas were rather isolated at that time. The selected trajectories illustrate the collapse of the forward conveyor and delineate the shallow and slow motion within the upper ocean layers.

Modeling of the Global Conveyor

Convection regime. The global ocean conveyor is weaker than in the regional NA experiments. The MWE data, in the amount suitable for setting the data up on a regular grid, exists only in a small region in the northern North Atlantic and the Nordic Seas (Sarnthein et al., 1995). The LGM salinity data over the entire globe is rather speculative if compared to the North Atlantic, where it is sufficient to form a data set on a regular grid (Duplessy et al., 1988). On the other hand, the

global simulations are far more advanced and physically consistent than any regional modeling because they give a continuous hydrodynamics of interconnected oceans without any need to introduce artificial sponge layers. Hence, it is a question of trade–off when one considers advantages and disadvantages of global versus regional modeling based on limited data. One definite advantage of global simulations is the presence of all major sources of deep water. The convection patterns (Figure 5) clearly delineate key differences in the dominant process of deep ocean ventilation in the northern and southern hemisphere at present and in the past. In Figure 5 the convection depth (the depth to which the convection due to hydrostatic instability penetrates) is shown as vertical bars. The deeper convection, the higher the bars (see legend in the diagrams). If multiplied by the area over which the convection occurred (here the surface of the grid cells), the depth of convection would represent the volume of convectively mixed water. Figure 5a indicates the dipole nature of deep ocean ventilation at present. The southern deep water sources around the Antarctic and particular in the Weddell and Ross Seas are counterbalanced by the northern NA source only, that is NADW balances AABW to form upper–to–deep ocean forward conveyor and deep–to–abyssal ocean reversed conveyor. Clearly, the LGM deep water production in the central NA, and reduced but still running convection in the Nordic Seas, led to somewhat curtailed but still running forward and abyssal reversed conveyors. The most important feature of the global HM and LGM forward conveyor is the coherent deep flow starting in the Nordic Seas and northern NA and flowing around the globe in the Antarctic Circumpolar Current with branches penetrating to the Indian and Pacific Oceans. Figure 5c implies that the deep ocean circulation must have changed radically because at MWE the bipolar convection regime was replaced by a regime with only southern deep ventilation. The whole northern NA and the Nordic Seas were convection–free at the MWE.

Figure 6 shows the present–day velocity vectors at 150 m (a) and 2500 m (b) depths. Figure 7 and Figure 8 depict the same for LGM and MWE respectively. A comparison of the MWE and HM and LGM deep ocean currents (Figure 6b, 7b, and 8b) indicates that the major change of the conveyor indeed took place at MWE, as the consideration of the convection regime implies. Here we concentrate on tracing the conveyor using the Lagrangian particles. As was mentioned above, these trajectories visualize the true three–dimensional water motion because they take into account both vertical motion and mixing in the convection chimneys. Since the vector maps suggest that the dramatic change of the conveyor took place at MWE rather than at LGM, we present the trajectories for the present day and MWE time slices only. Figure 9a shows two pairs of trajectories calculated using the modern velocity field and Figure 9b depicts the trajectories calculated using the MWE velocities. The particles to trace modern and MWE conveyor were deployed in different places. Two different sites were chosen because no deep convection has been found in the northern NA, whereas a site of deep convection exists southwest of Australia at both HM and MWE. However, only at MWE did particles deployed in the latter area progress westward and enter the central Atlantic. First, we briefly overview the OGCM results represented by velocity vectors and then emphasize how the semi–Lagrangian calculation enhances water transport analysis and understanding of the circulation change.

OGCM Results. The three–dimensional distribution of the horizontal currents is far more complex than Figures 5–7 display. The deep inflow of AABW into the central and North Atlantic is masked in these Figures. However, Figure 5 and 7 give a clear impression of how different the deep and upper ocean flows are. The present–day deep flows emerge as a truly global feature. This consolidated current system justifies, to a certain extent, the term ‘conveyor’. The upper ocean circulation system, however, does not give such an unambiguous impression of a continuous flow system. The intensive subtropical gyres are indeed connected by their marginal extensions to form a system that might have been recognized as connected rings of a chain comprising the upper band of the conveyor. It should be noted that because of the course resolution we cannot hope to model the correct operation of the upper band. For example, the Agulhas retroflection which would extend the leg of the Indian subtropical gyre into the South Atlantic can only be resolved in an eddy–resolving simulation. Nevertheless, one may say that no coherence comparable to the deep ocean conveyor structure can be found in the upper layers. Moreover, the water traveling in the uppermost levels is strongly modified by short–term air–sea interactions. The time scale of such interactions is about two to three months, which is an order of magnitude shorter than the time needed for water to travel around the globe within this circulation system. Since the water characteristics would change on that short–term time scale, the question of their origin as the conveyors’ water is therefore meaningless.

Because the structure of the glacial conveyor in the NA is not principally different from the modern one, the LGM conveyor is not illustrated here. Yet the glacial conveyor is characterized by a noticeable (here almost 60%) decrease in its intensity and the deep flows, especially in the NA, take different routes. Also, the NA conveyor branch became shallower than at present. However, as in Seidov et al. [1996], the NA conveyor still existed at the LGM. Since there was a weaker modern conveyor in the cited study, the relative changes are larger here (see above). The present–day overturning rate (here we ended up with 23 Sv) is perhaps an overestimate. We tried to obtain the convection in the northern NA that would penetrate deep enough (deeper than 2 km) by cooling the sea surface by 2°C (see above). The course resolution employed in this study led to an overestimate of the convective mixing and to overturning somewhat stronger than in other coarse resolution studies. The mediating estimate of the glacial to present–day overturning ratio is perhaps within 50% to 70%.

The major changes took place at the MWE. Although the impact is tied to the NGS and the northern NA only, the whole deep conveyor to the eastern Australian coast is affected. The NADW production was completely switched off, and

there is no deep southward flow in the western Atlantic. Moreover, the reversed deep ocean flow is found in these simulation to the north of a substantially curtailed deep ACC in the Indian and Atlantic sectors of the Southern Ocean. Although our calculations do not unambiguously indicate the reversal of the whole deep conveyor branch from the Atlantic to the northern Pacific, one may easily recognize that the deep flow has indeed an opposite direction over rather a long leg from the eastern Indian ocean to the northern NA. Additionally, a clearly seen deep southward–flowing western boundary current developed in the northern Pacific (Figure 8b). This flow, which is absent from the present day deep current system, is a signature of the possibly reversed Pacific branch of the global conveyor.

Trajectory tracing. We have already emphasized above that the horizontal velocity vectors, even if inspected at each level, may be misleading because they do not show vertical motion. It is especially true in the areas of convection where water is mixed vertically and particles may be transferred to the deep ocean. Hence, the true 3–D motion would be essentially different from what the vector maps might have suggested. To illuminate the deep ocean ventilation and subsequent water transport by the conveyor, the particles were deployed in the areas where they can be transferred to the deep ocean within convection chimneys to trace the deep ocean conveyor leg.

Some of the particles deployed in the NGS and northern NA penetrated into the deep ocean and traveled southward in the western boundary current (Figure 9a). Some of these particles pass further into the South Atlantic, although many remained trapped in the NA subtropcal gyre. Some of those which manage to travel to the South Atlantic turn backward. About 10% to 20% of all particles deployed in the shaded area in Figure 5a reached the ACC and were transported further eastward in this current. Only 2% to 5% of these particles ever emerged in the northern Pacific. Hence, this study indicates that only a tiny fraction of the NADW can physically travel along the whole leg of the deep conveyor. However, it does not mean that the NADW water cannot reach the Pacific in significant amounts. One must consider the duration of the process which can be of several thousand years of a stable modern–like conveyor. Some additional calculations that combine the lagrangian technique with incorporation of geochemical tracers are required to quantify the total amount of NADW reaching the northern Pacific at the slow rate indicated by our experiments (no more than 1–2 Sv in the model).

In spite of uncertainties in our present day calculations due to a rather coarse horizontal resolution and a somewhat incomplete glacial and meltwater sea surface climatology, the MWE curtailment of the conveyor and emergence of the reversed deep conveyor is a very robust feature. In many additional experiments with additional disturbances of MWE sea surface conditions, a switched off or even reversed NA conveyor was a permanent feature. All attempts to find a trajectory originating somewhere in the NA and continuing into at least the Indian Ocean have failed. On the contrary, the particles deployed at the surface to the southwest of Australia travel far into the South Atlantic. A tiny fraction of the deployed ensemble was found north of the equator. However, no particles managed to pass into the northern NA. Hence, although there was indeed a strong incursion of the AABW into the NA it upwelled mostly to the south of 50°N, which agrees well with the results of Seidov et al. (1996) who show isopycnal outcrop to the south of 50°N. Such a southward–shifted density outcrop isolated the northern NA from the rest of the World Ocean. Hence, the main driving mechanism of the deep ocean circulation during MWE was restricted to the Southern Ocean.

Discussion and Conclusions

The primary task of our paper is to demonstrate that the major meltwater events in the NA might have affected the deep ocean branch of the global conveyor very substantially and that these changes can be clearly and unambiguously traced in Lagrangian calculations. The characteristics of ocean circulation, such as the ventilation of the deep ocean, sedimentation transport, water parcel motion, meridional overturning and potential vorticity analysis, all indicate a weakening and some shallowing of the main conveyor at the LGM. These characteristics indicate a complete collapse after the very localized freshwater discharge at the MWE occurred. This may be instrumental for understanding and predicting global climate change on the basis of the top–analog examples given by the major deglaciations. Our results also demonstrate, not only in an idealized sensitivity simulation, but based on numerous proxy data, that the deep ocean circulation is indeed sensitive to localized high–latitudinal forcing that might be able to destroy water convection in the World Ocean.

The lagrangian calculations help to elaborate the true three–dimensional water motion and therefore are the only means by which conveyor modes can be genuinely visualized. Moreover, the trajectory–tracing technique may indicate whether specific parts of the global ocean are inter–connected via the deep conveyor branches, or essentially isolated. For example, the northern NA during the MWE is characterized by very old nonventilated intermediate–to–deep water (Sarnthein et al., 1995). Our calculations may shed some additional light on this problem. If the MWE water in the NA was a mixture of the AABW, originating in the Weddell Sea and some water sinking in the eastern Indian ocean, it may explain extreme aging of the Atlantic water, stronger than it would be if only the AABW ventilated the NA areas.

A combined circulation/sedimentation/particle tracing modeling approach was employed to understand particular aspects of the glacial–interglacial change of the North Atlantic and World Ocean circulation which are difficult to address using single–component models. Primary among those are the ventilation regimes, including the characterization of vertical mixing in convective chimneys and the advective ages of ventilated water. Circulation studies might focus on the NADW outflow or deep ocean circulation routing. Most of these questions are traditionally addressed using geochemical tracers such as $\delta^{18}O$, $\delta^{13}C$, and $\Delta^{14}C$, which are extremely useful in ocean circulation studies and hence widely employed.

However, the tracers alone cannot provide sufficient constraints over a simulated past circulation, as has been shown recently by LeGrand and Wunsch [1995]. In their study they showed that there exist an infinite number of states that would satisfy a tracer distribution aimed at constraining the circulation, at least for the currently available proxy data sets.

Another problem arising in paleoceanographic investigations is the parallel analysis of both surface and benthic habitats and/or sediment transport features. Commonly, assumed features of a water flow thought to be suitable for explaining a particular distribution of proxy data are largely based on speculation. There is no guarantee that this hypothetical flow would satisfy hydrodynamic restrictions posed over the ocean by the wind stress, ocean geometry, bottom morphology, and sea surface heat and fresh water fluxes.

Based on only partly known SSS, recently corrected SST, and simulated glacial wind stress, our results largely conform to current ideas about ventilation and overturn in the North Atlantic at the height of the last glaciation and during the subsequent meltwater event near 13 500 ^{14}C years B.P. The sediment transport model output contains features that agree well with interpretation of sediment data in the northern North Atlantic. In Seidov and Haupt [1997] we discussed the LGM sedimentation pattern resulting from our simulation in comparison with the observed or inferred data of Cremer et al. [1993] and McCave and Tucholke [1986]. It was pointed out that our simulations are in good qualitative agreement with their findings. Moreover, in our experiments, the sediment load in the vicinity of the North American coast is lower during the LGM than today, in agreement with the interpretation given by Boyle and Keigwin [1987] on the basis of nutrient concentration analysis. The Caribbean water at depths just above 2 km was nutrient depleted during the glacial period. One interpretation is that there was a lower proportion of northern component water, which in turn means a weaker deep western boundary current and a stronger southern source water incursion.

In the eastern part of the NA, our sediment model agrees with data that indicate increased flow along the eastern flank of the Mid–Atlantic Ridge. Dowling and McCave [1993] and Robinson and McCave [1994] provide evidence that the Feni Drift was substantially enhanced at the last glacial maximum. Generally, the glacial sediment record indicates an enhanced Holocene bottom current driven by the Iceland–Greenland overflow characteristic of modern NADW production in the Norwegian–Greenland Seas.

Our trajectory–tracing model reveals very different fates of the water volumes in the HM and LGM cases, once exposed to the air–sea interaction and then mixed downward in convective chimneys. NADW production in the center of the glacial North Atlantic is strongly supported by the proxy data [Duplessy at al., 1988, 1991; Sarnthein et al., 1994, 1995]. In general, the most recent studies indicate enhanced upper NADW production and decreased lower NADW production [e.g., Oppo et al., 1995]. However there exists evidence that, despite decreased lower NADW production, the glacial conveyor was not, in total, weaker than today [Yu et al., 1996]. This may appear contradictory to the fact that the glacial northward heat transport was substantially weaker at the LGM. Our trajectory analysis explains this seemingly controversial result. It shows that although the forward conveyor, responsible for meridional heat transport, became weaker, the abyssal reversed branch of the conveyor strength increased proportionally to allow the same rate of the southward transport of the tracers in the deep ocean found by Yu et al. [1996]. Mediating the results of Seidov et al. [1996], Seidov and Haupt [1997] and the global conveyor simulations presented above, one may give the ratio of LGM to HM conveyor intensity to be within 50%–70% of modern magnitude.

Duplessy et al. [1988] argue that during glacial times most of the deep eastern North Atlantic was filled with southern source water which probably penetrated up to 45°N. Our experiments, deploying particles in the surface layers in the subpolar gyre and in the deep and abyssal areas in the subtropical gyre, are in complete agreement with this conclusion. Moreover, Michel et al. [1995] point to a steep gradient in d13C distribution northward of 30°N in the North Atlantic delineating the border between southern and northern source water at the LGM. We add that this border probably shifted farther to the north in the eastern part of the basin during that time period.

Moreover, we point out that the trajectory analysis is in agreement with the notion of a far better ventilated and deeper glacial thermocline in the subtropical North Atlantic [Slowey and Curry, 1995]. These authors provide indications that the glacial thermocline was shallower than today with its base raised by about 100 m. However, the water inside the glacial thermocline was up to 4°C cooler than today. Our Figure 3 confirms that the glacial thermocline was better ventilated and that there was an enhanced production of subtropical mode water. Deeper glacial ventilation, evident in Plate 2d, implies that the base of thermocline had to rise upward because water pumped into the thermocline was more than 4°C colder at the glacial ventilation points (westward boundary outflow region; compare Figure 3a and 3b). To quantify this effect, the difference between today's and the LGM simulated temperature is shown in a meridional section of the temperature anomaly field in Figure 8. In essence, Figure 8 displays a penetration of cold anomalies deep into the thermocline. It is clear, however, that this penetration is limited to the upper 1 km and that the lower 500 m of this layer is more strongly cooled than the upper 500 m. This implies that the thermocline base has been raised. A comparison of the temperature profiles in the subtropical gyres indicates that on average the thermocline depth was about 200 m shallower than today, which differs from the estimates of Slowey and Curry [1995]. There may be several reasons for this discrepancy. Firstly, the subtropical gyre is dangerously close to the sponge layer at the southern wall, which might have distorted the behavior of the thermocline base. Second, we use the annual mean surface forcing and, therefore, we are unable to simulate an

extreme winter southward migration of the density outcrop intersecting the Ekman pumping within the subtropical gyre. Nevertheless, the general tendencies sketched in Figure 1 of Slowey and Curry [1995, p. 717] are evident in our trajectory maps (Plate 2d as compared to Plate 2c). The particles dive deeper into the thermocline and stay there longer. The northern limit of the subtropical gyre, marked by the shallow convection along the North Atlantic Drift, is shifted noticeably southward.

As some findings have indicated [e.g., Sarnthein et al., 1995], the Nordic Seas were more isolated from the northern North Atlantic at the LGM than today. This is strongly supported by our Lagrangian calculations. As Figure 7 displays, the water from the subtropics probably had a very limited chance to enter the Nordic Seas, largely because the outflow over the Iceland–Greenland Ridge was reduced during the LGM.

Based on a threefold numerical simulation of the North Atlantic circulation and sedimentation and twofold simulation of the World Ocean water transport we draw the following conclusions:

1. Present day and LGM meridional thermohaline circulation is characterized by a forward global deep ocean conveyor. At MWE the freshwater fluxes that maintain the `observed' high latitudinal sea surface salinity appear to be sufficient to suppress this forward conveyor. A reversed deep ocean conveyor replaced the forward one on the whole distance from NA to the southeast Indian Ocean.

2. The convection regime is the most crucial process for the conveyor dynamics. At MWE bimodal convection regime, with both NADW and AADW sources, was replaced by the regime with only southern deep water source driving the conveyor. As a result, a reversed conveyor emerged in the Indian–Atlantic sector of the Southern Ocean. The meltwater North Atlantic was essentially isolated from the other parts of the World Ocean.

3. Sedimentation in the North Atlantic is non–linearly coupled to the circulation modes associated with different surface climatology. The LGM and MWE sedimentation patterns differ fundamentally from the Holocene/Modern pattern in a way that cannot be expected a priori. The major differences indicated by sediment transport and trajectory–tracing models are summarized in following conclusions.

4. The results of sediment transport model suggest that there was almost no sediment deposition in the Gulf Stream area, and a lower rate than at present in the Caribbean during MWE.

5. The trajectory–tracing model indicates far stronger ventilation of the thermocline in the glacial low latitudes than is observed today. The trajectory–tracing model indicates complete absence of the deep ocean ventilation at the MWE. The model reveals disappearance of the deep western boundary current and westward contraction of the subtropical warm pool. This contraction leads to collapse of the eastern continuation of the North Atlantic drift and contributes to formation of the upper ocean reverse conveyor.

6. Concerning the use of numerical models as a principal source of sediment transport and Lagrangian calculations, it should be stressed that at high latitudes the sediment transport and water–volume tracing models can only operate with the simulated rather than observed circulation patterns. The water transport calculations depend critically on knowledge about where the convection occurs and how deep it ventilates.

Acknowledgments. This study could not have been carried out without the efforts invested by the Kiel group into paleoreconstructions of the glacial–interglacial North Atlantic. We are especially grateful to Michael Sarnthein for inspiring us to study the meltwater oceanography using the reconstructions provided by the Kiel group and Karl Stattegger for the support and helpful comments. We deeply appreciate Avan Antia's help on correcting our English. The study was accomplished within the framework of the German Climate Program and supported by the Deutsche Forschungsgemeinschaft (DFG) and SFB313 of Kiel University.

References

Bard, E., F. Rostek, and C. Sonzogni, Interhemispheric synchrony of the last deglaciation inferred from alkenone palaeothermometry, Nature, 385, 707–710, 1997.

Beck, J. W., J. Récy, F. Taylor, R. L. Edwards, and G. Cabioch, Abrrupt changes in early Holocene tropical sea surface temperature derived from coral records, Nature, 385, 705–707, 1997.

Beveridge, N. A. S., H. Elderfield, and N. J. Shackleton, Deep thermohaline circulation in the low–latitude Atlantic during the last glacial, Paleoceanography, 10, 643–660, 1995.

Bitzer, K., and R. Pflug, DEPOD: A three–dimensional model for simulating clastic sedimentation and isostatic compensation in sedimentary basin, in Quantitative Dynamics Stratigraphy, edited by T. A. Cross, pp. 335–348, Prentice Hall, New York, 1990.

Bohrmann, G., R. Henrich, and J. Thiede, Miocene to Quaternary paleoceanography in the northern North Atlantic: Variability in carbonate and biogenic opal accumulation, in Geological History of the Polar Oceans: Arctic Versus Antarctic, edited by U. Bleil and J. Thiede, pp. 647–675, Kluwer Acad., Norwell, Mass., 1990.

Bond, G. C., Climate and conveyor, Nature, 377, 383–384, 1995.

Bond, G.et al., Evidence for massive discharges of icebergs into the North Atlantic Ocean during the last glacial period, Nature, 360, 245–249, 1992.

Böning, C. W., and M. D. Cox, Particle dispersion and mixing of conservative properties in an eddy–resolving model, J. Phys. Oceanogr., 18, 320–338, 1988.

Böning, C. W., R. Döscher, and R. G. Budich, Seasonal transport in the western North Atlantic: Experiments with an eddy–resolving model, J. Phys. Oceanogr., 21, 1271–1289, 1991.

Boyle, E., Deep water distillation, Nature, 379, 679–680, 1996.

Boyle, E. A., and L. D. Keigwin, North Atlantic thermohaline circulation during the past 20,000 years linked to high–latitude surface temperature, Nature, 330, 35–40, 1987.

Boyle, E., and A. Weaver, Conveying past climates, Nature, 372, 41–42, 1994.

Broecker, W., The great ocean conveyor, Oceanography, 4, 79–89, 1991.

Broecker, W. S., and G. H. Denton, The role of ocean atmosphere reorganizations in glacial cycles, Geochim. Cosmochim. Acta, 53, 2465–2501, 1989.

Bryan, F., High–latitude salinity effects and interhemispheric thermohaline circulations, Science, 323, 301–304, 1986.

Bryan, F., Parameter sensitivity of primitive equation ocean general circulation models, J. Phys. Oceanogr., 17, 970–985, 1987.

Bryan, F., and W. Holland, A high resolution simulation of the wind– and themohaline–driven circulation in the North Atlantic Ocean, in Parameterization of Small–Scale Processes, edited by P. Müller and D. Henderson, pp. 99–115, Hawaii Inst. of Geophys., Honolulu, 1989.

Bryan, K., A numerical method for the study of the circulation of the world ocean, J. Comput. Phys., 4, 347–376, 1969.

Climate: Long–Range Investigation Mapping and Prediction (CLIMAP) Project Members, Seasonal reconstructions of the Earth's surface at the last glacial maximum, Map and Chart Ser. MC–36, pp. 1–18, Geol. Soc. of Am., Boulder, Colo., 1981.

Colin de Verdière, A., Buoyancy driven planetary flows, J. Mar. Res., 46, 215–265, 1988.

Cox, M. D., A primitive equation, 3–dimensional model of the ocean, Tech. Rep. No. 1, 250 pp., Ocean Group, Geophys. Fluid Dyn. Lab., Princeton, Univ., Princeton, N.J., 1984.

Cox, M., An idealized model of the world ocean, I, The global–scale water masses, J. Phys. Oceanogr., 19, 1730–1752, 1989.

Cox, M., and K. Bryan, A numerical model of the ventilated thermocline, J. Phys. Oceanogr., 14, 674–687, 1984.

Cremer, M., J.–C. Faugeres, F. E. Grousset, and E. Gonthier, Late Quaternary sediment flux on sedimentary drifts in the northeast Atlantic, Sediment. Geol., 82, 89–101, 1993.

Dowling, L. M., and I. N. McCave, Sedimentation on the Feni drift and late Glacial bottom water production in the northern Rockall Trough, Sediment. Geol., 1993, 79–87, 1993.

Drijfhout, S. S., E. Maier–Reimer, and U. Mikolajewicz, Tracing the conveyor belt in the Hamburg large–scale geostrophic ocean general circulation model, J. Geophys. Res., 101, 22,563–22,575, 1996.

Duplessy, J.–C., and N. J. Shackleton, Response of global deep–water to Earth’s climate change 135,000–107,000 years ago, Nature, 316, 500–507, 1985.

Duplessy, J.–C., N. J. Shackleton, R. G. Fairbanks, L. Labeyrie, D. Oppo, and N. Kallel, Deepwater source variations during the last climatic cycle and their impact on the global deepwater circulation, Paleoceanography, 3, 343–360, 1988.

Duplessy, J.–C., L. Labeyrie, A. Julliet–Lerclerc, J. Duprat, and M. Sarnthein, Surface salinity reconstruction of the North Atlantic Ocean during the last glacial maximum, Oceanol. Acta, 14, 311–324, 1991.

Einsele, G., Sedimentary Basins; Evolution, Facies, and Sediment Budget, pp. 628, Springer–Verlag, New York, 1992.

England, M. H., Representing global–scale water masses in ocean general circulation models, J. Phys. Oceanogr., 23, 1523–1552, 1993.

Fichefet, T., and S. Hovine, The glacial ocean: A study with a zonally averaged, three–basin ocean circulation model, in Ice in Climate System, NATO ASI Ser., Ser. I, 12, edited by W. R. Peltier, pp. 433–458, Springer–Verlag, New York, 1993.

Fichefet, T., S. Hovine, and J.–C. Duplessy, A model study of the Atlantic thermohaline circulation during the last glacial maximum, Nature, 372, 252–255, 1994.

Goldschmidt, P., Accumulation rates of coarse–grained terrigenous sediment in the Norwegian–Greenland Sea: Signals of continental glaciation, Mar. Geol., 128, 137–151, 1995.

Goldschmidt, P. M., S. Pfirmann, I. Wollenburg, and R. Henrich, Origin of sediment pellets from the Arctic seafloor. Sea ice or icebergs?, Deep Sea Res., 372, 252–255, 1992.

Gordon, A., Interocean exchange of thermocline water, J. Geophys. Res., 91, 5037–5046, 1986.

Gordon, A. L., S. E. Zebiak, and K. Bryan, Climate variability and the Atlantic Ocean, Eos Trans. AGU, 73, 161, 164–165, 1992.

Guilderson, T. P., R. G. Fairbanks, and Rubenstone, J. L., Tropical Temperature Variations Since 20,000 Years Ago: Modulating Interhemispheric Climate Change, Science, 263, 663–664, 1994.

Hasselmann, K., An ocean model for climate variability studies, Prog. in Oceanogr., 11, 69–92, 1982.

Haupt, B. J., Numerische Modellierung der Sedimentation im nördlichen Nordatlantik, Ber. 54, pp. 1–129, Sonderforschungsbereich 313, Univ. Kiel, Kiel, Germany, 1995.

Haupt, B. J., C. Schäfer–Neth, and K. Stattegger, Modeling sediment drifts: A coupled oceanic circulation–sedimentation model of the northern North Atlantic, Paleoceanography, 9, 897–916, 1994.

Haupt, B. J., C. Schäfer–Neth, and K. Stattegger, Three–dimensional numerical modeling of late Quaternary paleoceanography and sedimentation in the northern North Atlantic, Geol. Rundsch., 84, 137–150, 1995.

Honjo, S., Particle fluxes and modern sedimentation in the polar oceans, in Polar Oceanography, Part B, edited by W. O. Smith, pp. 687–739, Academic, San Diego, Calif., 1990.

Hsü, K. J., Physical Principles of Sedimentology, pp. 231, Springer–Verlag, New York, 1989.

Keigwin, L. D., G. Jones, and S. J. Lehman, Deglacial meltwater discharge, North Atlantic deep circulation, and abrupt climate change, J. Geophys. Res., 96, 16811–16826, 1991.

Kellogg, T. B., Paleoclimatology and paleo–oceanography of the Norwegian and Greenland Seas; Glacial–interglacial contrasts, Boreas, 9, 115–137, 1980.

Killworth, P. D., Deep convection in the world ocean, Rev. Geophys., 21, 1–26, 1983.

Kroopnick, P. M., The distribution of 13C and ΣCO2 in the world oceans, Deep Sea Res., 32, 57–84, 1985.

Lautenschlager, M., and K. Herterich, Atmospheric response to ice age conditions — Climatology near the Earth's surface, J. Geophys. Res., 95, 22,547–22,557, 1990.

LeGrand, P., and K. Wunsch, Constraints from paleotracer data on the North Atlantic circulation during the last glacial maximum, Paleoceanography, 10, 1011–1045, 1995.

Lehman, S. J., and L. D. Keigwin, Sudden changes in North Atlantic circulation during the last deglaciation, Nature, 356, 757–762, 1992.

Levitus, S., Climatological atlas of the world ocean, NOAA Prof. Pap., 13, 173 pp., U.S. Govt. Print. Off., Washington, D.C., 1982.

Levitus, S., and T. P. Boyer, World Ocean Atlas 1994, vol. 4, (Temperature; 117 pp.), NOAA Natl. Environ. Satell. Data and Inf. Ser., Washington, D.C., 1994.

Levitus, S., R. Burgett, and T. P. Boyer, World Ocean Atlas 1994, vol.3, (Salinity; 99 pp.) NOAA Natl. Environ. Satell. Data and Inf. Ser., Washington, D.C., 1994.

Lorenz, S., B. Grieger, P. Helbig, and K. Herterich, Investigating the sensivity of the atmospheric general circulation Model ECHAM 3 to paleoclimate boundary conditions, Geol. Rundsch., 85, 513–524, 1996.

Luyten, J. R., J. Pedlosky, and H. Stommel, The ventilated thermocline, J. Phys. Oceanogr., 13, 292–309, 1983.

Maier–Reimer, E., and U. Mikolajewicz, Experiments with an OGCM on the cause of the Younger Dryas, Rep. 39, 13 pp., Max–Plank–Inst. für Meteorol., Hamburg, Germany, 1989.

Maier–Reimer, E., U. Mikolajewicz, and K. Hasselmann, On the sensitivity of the global ocean circulation to changes in the surface heat flux forcing , Rep. 68, 67 pp., Max–Plank–Inst. für Meteorol., Hamburg, Germany, 1991.

Maier–Reimer, E., U. Mikolajewicz, and K. Hasselmann, Mean circulation of the Hamburg LSG OGCM and its sensitivity to the thermohaline surface forcing, J. Phys. Oceanogr., 23, 731–757, 1993.

Manabe, S., and R. J. Stouffer, Two stable equilibria of a coupled ocean–atmospher model, J. Clim., 1, 841–866, 1988.

Manabe, S., and R. J. Stouffer, Simulation of abrupt change induced by freshwater input to the North Atlantic Ocean, Nature, 378, 165–167, 1995.

Marotzke, J., and J. Willebrand, Multiple equilibria of the global thermohaline circulation, J. Phys. Oceanogr., 21, 1372–1385, 1991.

Maslin, M. A., N. J. Shackleton, and U. Pflaumann, Surface water temperature, salinity, and density changes in the northeast Atlantic during the last 45,000 years: Heinrich events, deep water formation, and climatic rebounds, Paleoceanography, 10, 527–544, 1995.

McCartney, M. S., Recirculating components to the deep boundary current of the nothern North Atlantic, Prog. in Oceanogr., 29, 283–383, 1992.

McCave, I. N., and B. E. Tucholke, Deep current controlled seimentation in the western North Atlantic, in The Geology of North America, vol. M. The Western North Atlantic Region, edited by P. R. Vogt and B. E. Tucholke, pp. 451–468, Geol. Soc. of Am., Boulder, Colo., 1986.

Michel, E., L. D. Labeyrie, J.–C. Duplessy, N. Gorfti, M. Labracherie, and J.–L. Turon, Could deep Subantarctic convection feed the world deep basins during the last glacial maximum?, Paleoceanography, 10, 927–942, 1995.

Mikolajewicz, U., A meltwater induced collapse of the 'conveyor belt' themohaline circulation and its influence on the distribution of Δ14C and δ18O in the oceans, Rep. 189, 25 pp., Max–Plank–Inst. für Meteorologie, Hamburg, Germany, 1996.

Miller, M. C., I. N. McCave, and P. D. Komar, Threshold of sedimentation under unidirectional currents, Sedimentol., 24, 507–528, 1977.

Oppo, D. W., and S. J. Lehman, Mid–depth circulation of the subpolar north Atlantic during the last glacial maximum, Science, 259, 1148–1152, 1993.

Oppo, D. W., M. E. Raymo, G. P. Lohmann, A. C. Mix, J. D. Wright, and W. L. Prell, A δ13C record of Upper North Atlantic Deep Water during the past 2.6 million years, Paleoceanogr., 10, 373–394, 1995.

Pacanowski, R., K. Dixon, and A. Rosati, The GFDL modular ocean users guide, Tech. Rep. 2, Ocean Group, Geophys. Fluid Dyn. Lab., Princeton Univ., Princeton, N. Y., 1993.

Pfirmann, S., M. A. Lange, I. Wollenburg, and P. Schlosser, Sea ice characteristics and the role of sediment inclusions in deep–sea deposition: Arctic – Antarctic comparisons, in Geological History of the Polar Oceans: Arctic Versus Antarctic, edited by U. Bleil and J. Thiede, pp. 187–211, Kluwer Acad., Norwell, Mass., 1990.

Puls, W., Numerical simulation of bedform mechanics. Mitteilungen des Inst. für Meeresk. Univ. Hamburg, Hamburg, Germany, 147 pp., 1981.

Rahmstorf, S., Rapid climate transitions in a coupled ocean–atmosphere model, Nature, 372, 82–85, 1994.

Rahmstorf, S., Bifurcations of the Atlantic thermohaline circulation in response to changes in the hydrological cycle, Nature, 378, 145–149, 1995.

Robinson, S. G., and I. N. McCave, Orbital forcing of bottom–current enhanced sedimentation on Feni Drift, NE Atlantic, during the mid–Pleistocene, Paleoceanography, 9, 943–972, 1994.

Ruddiman, W. F., and A. McIntyre, The mode and mechanism of the last deglaciation: Oceanic evidence., Quat. Res., 16, 125–134, 1981.

Sakai, K., and W. R. Peltier, A simple model of the Atlantic thermohaline circulation: Internal and forced variability with paleoclimatological implications, J. Geophys. Res., 100, 13,455–13,479, 1995.

Sarmiento, J. L., On the north and tropical Atlantic heat balance, J. Geophys. Res., 91, 11,677–11,689, 1986.

Sarnthein, M., K. Winn, S. J. A. Jung, J.–C. Duplessy, L. Labeyrie, H. Erlenkeuser, and G. Ganssen, Changes in east Atlantic deepwater circulation over the last 30,000 years — eight time slice reconstructions, Paleoceanography, 9, 209–267, 1994.

Sarnthein, M. et al., Variations in Atlantic Ocean paleoceanography, 50°–80°N: A time slice record of the last 30,000 years, Paleoceanography, 10, 1063–1094, 1995.

Schmitz, W. J., Jr., On the interbasin–scale thermohaline circulation, Rev. Geophys., 33, 151–173, 1995.

Schulz, H., Meeresoberflächentemperaturen im frühen Holozän 10,000 Jahre vor heute, Ph.D. dissertation, Univ. Kiel, Kiel, Germany, 1994.

Seibold, E., and W. H. Berger, The Sea Floor; An Introduction to Marine Geology, 2nd ed., Springer–Verlag, New York, 1993.

Seidov, D. G., Numerical modeling of the ocean circulation and paleocirculation, Mesozoic and Cenozoic Oceans, Geodyn. Ser., vol.15, edited by K. J. Hsu, pp. 11–26, AGU, Washington, D. C., 1986.

Seidov, D., An intermediate model for large–scale ocean circulation studies, Dyn. Atmos. Oceans, 25/1, 25–55, 1996.

Seidov, D., and R. Prien, A coarse resolution North Atlantic ocean circulation model: An intercomparison study with a paleoceanographic example, Ann. Geophys., 14, 246–257, 1996.

Seidov, D., and B. J. Haupt, Simulated ocean circulation and sediment transport in the North Atlantic during the last glacial maximum and today, Paleoceanography, 12, No. 2, 281–305, 1997.

Seidov, D., M. Sarnthein, K. Stattegger, R. Prien, and M. Weinelt, North Atlantic ocean circulation during the last glacial maximum and subsequent meltwater event: A numerical model, J. Geophys. Res., 101, 16,305–16,332, 1996.

Semtner, A. J., Finite difference formulation of a world ocean model, in Advanced Physical Oceanographic Modelling, edited by J. O'Brien, pp. 187–202, D. Reidel, Norwell, Mass. 1986.

Send, U., and J. Marshall, Integral effects of deep convection, J. Phys. Oceanogr., 25, 855–872, 1995.

Shanks, A. L., and J. D. Trent, Marine snow: Sinking rates and potential role in vertical flux, Deep Sea Res., Part A, 27, 137–143, 1980.

Shapiro, R., The use of linear filtering as a parameterization of atmospheric diffusion, J. Atmos. Sci., 28, 523–531, 1971.

Slowey, N. C., and W. B. Curry, Enhanced ventilation of the North Atlantic subtropical gyre thermocline during the last glaciation, Nature, 358, 665–668, 1992.

Slowey, N. C., and W. B. Curry, Glacial–interglacial differences in circulation and carbon cycling within the upper western North Atlantic, Paleoceanography, 10, 715–732, 1995.

Stocker, T. F., The variable ocean, Nature, 367, 221–222, 1994.

Stommel, H., and A. B. Arons, On the abyssal circulation of the world ocean, II, An idealized model of the circulation pattern and amplitude in the oceanic basins, Deep Sea Res., 6, 217–233, 1960.

Stull, R. B., Transilient turbulence theory, I, The concept of eddy–mixing across finite distances, J. Atmos. Sci., 41, 3351–3367, 1984.

Sündermann, J., North Sea Dynamics, Dynamics, edited by J. Sünderman and W. Lenz , 693 pp., Springer–Verlag, New York, 1983.

Sündermann, J., and R. Klöcker, Sediment transport modeling with applications to the North Sea, in North Sea Dynamics, pp. 453–471, Springer–Verlag, New York, 1983.

Syvitski, J. P. M., and T. M. C. Hughes, Delta 2: Delta progadation and basin filling, Comput. Geosci., 18, 839–897, 1992.

Tetzlaff, D. N., and J. W. Harbaugh, Simulating Clastic Sedimentation, Van Nostrand Reinhold, New York, 1989.

Toggweiler, J. R., K. Dixon, and K. Bryan, Simulations of radiocarbon in a coarse–resolution world ocean circulation model, 1, Steady state prebomb distribution, J. Geophys. Res., 94, 8217–8242, 1989.

Weaver, A. J., and T. M. C. Hughes, Rapid interglacial climate fluctuations driven by North Atlantic ocean circulation, Nature, 367, 447–450, 1994.

Weaver, A. J., and E. S. Sarachik, The role of mixed boundary conditions in numerical models of the ocean's climate, J. Phys. Oceanogr., 21, 1470–1492, 1991.

Weaver, A. J., J. Marotzke, P. F. Cummins, and E. S. Sarachik, Stability and variability of the thermohaline circulation, J. . Phys. Oceanogr. , 23, 39–60, 1993.

Webb, R. S., D. H. Rind, Scott J. Lehman, R. J. Healy, and D. Sigman, Influence of ocean heat transport on the climate of the Last Glacial Maximum, Nature, 385, 695–699.

Weinelt, M., Veränderungen der Oberflächenzirkulation im Europäischen Nordmeer während der letzten 60.000 Jahre – Hinweise aus stabilen Isotopen, Ber. 41, pp. 1–106, Sonderforschungsbereich 313, Univ. Kiel, Kiel, Germany, 1993.

Wold, C. N., Paleobathymetry and sediment accumulation in the northern North Atlantic and southern Greenland–Iceland–Norwegian Sea, Ph.D. thesis, Univ. of Kiel, Kiel, Germany, 1992.

Wright, D., and T. F. Stocker, A zonally averaged ocean model for the thermohaline circulation, I, Model development and flow dynamics, J. Phys. Oceanogr., 21, 1713–1724, 1991.

Yu, E.–F., R. Francois, and M. P. Bacon, Similar rates of modern and last–glacial ocean thermohaline circulation inferred from radiochemical data, Nature, 379, 689–694, 1996.

Zanke, U., Zusammenhänge zwischen Strömung und Sedimenttransport, Teil 1, Berechnung des Sedimenttransports — allgemeiner Fall —, Mitt. Franzius Inst. Wasserbau Küsteningeneuerswesen Tech. Univ. Hannover, 47, 214–345, 1978.

Zhang, S., C. Lin, and R. J. Greatbatch, A thermocline model for ocean–climate studies, J. Mar. Res., 50, 99–124, 1992.

Table 1. Surface Data Sources for Different Time Slices in the Numerical Experiments

Data \ Time	Modern/Holocene	LGM (18,000–15,000 ^{14}C yr B.P.)	MWE (14,200–13,200 ^{14}C yr B.P.)
Wind stress	T42 wind stress	T42 wind stress calculated using *CLIMAP* [1981] surface conditions (*Lorenz et al.* [1996]	as for LGM
Sea surface temperature (SST)	*Levitus* [1982] and *Dietrich* [1969] in the NGS (see text and Figure 1)	*CLIMAP* [1981] and LGM data of *Schulz* (1994) and data of *Sarnthein et al.* [1992,1995] in the northern NA and NGS	*CLIMAP* [1981] and data of *Schulz* [1994] in the northern NA and NGS
Sea surface salinity (SSS)	*Levitus* [1982] and *Dietrich* [1969] in the NGS (see text)	*Levitus* [1982] south of 40°N and recalculated SSS using δ^{18}O from *Duplessy et al.* [1991] north of 40°N, and *Sarnthein et al.* [1995] north of 50°N in the northern NA and NGS for LGM (see Figure 1)	LGM SSS and recalculated SSS using δ^{18}O data of *Sarnthein et al.* [1995]in the northern NA and NGS for MWE north of 50°N

Abbreviations are LGM, last glacial maximum; MWE, meltwater event; NA, North Atlantic; NGS, Norwegian–Greenland Seas. The data in the NA are combined with the modified present–day sea surface climatology to provide the basis for the global ocean modeling (see text)

Captions

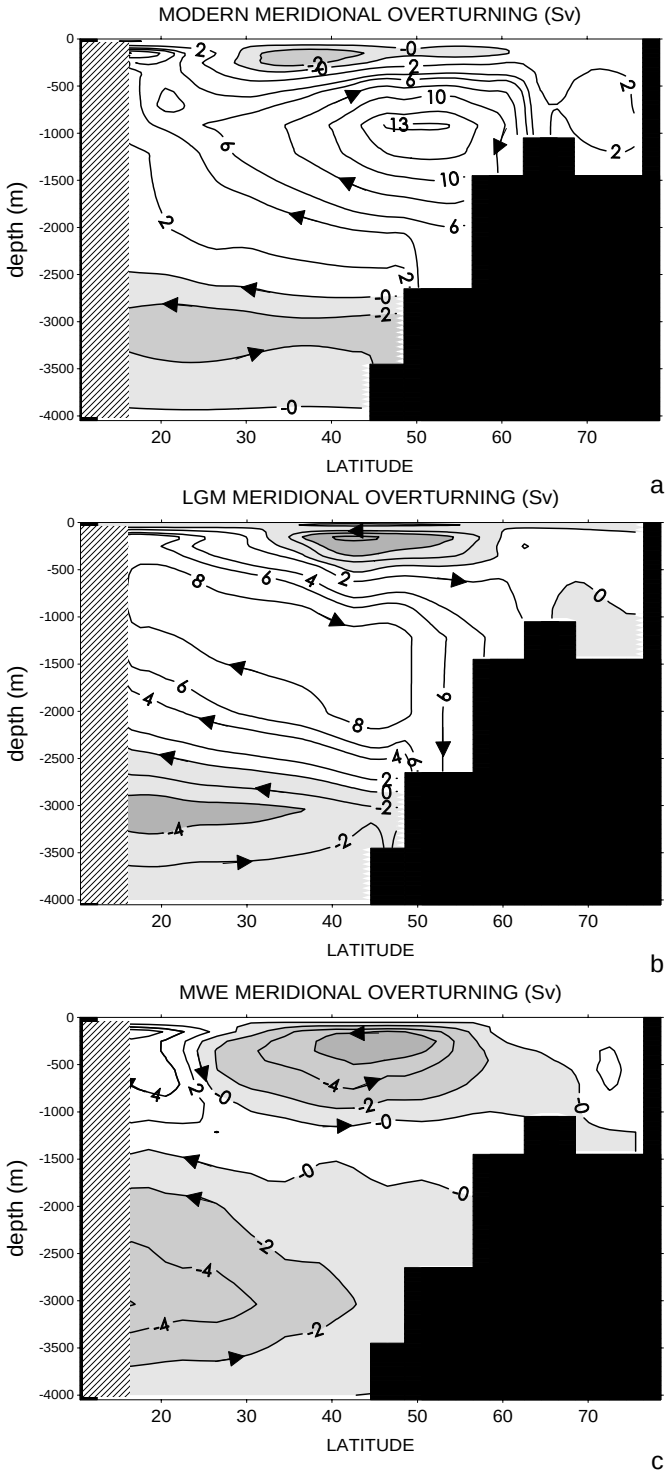

Figure 1

Figure 1. Overturning stream function showing total meridional transport in the North Atlantic (in Sv; $1Sv=10^6\ m^3s^{-1}$): a) present-day overturning pattern; b) LGM; c) MWE. The patterns within the sponge layer at the southern boundary (see text) are masked. Areas of negative values are shaded. Arrows show direction of the transport (after Seidov et al., 1996).

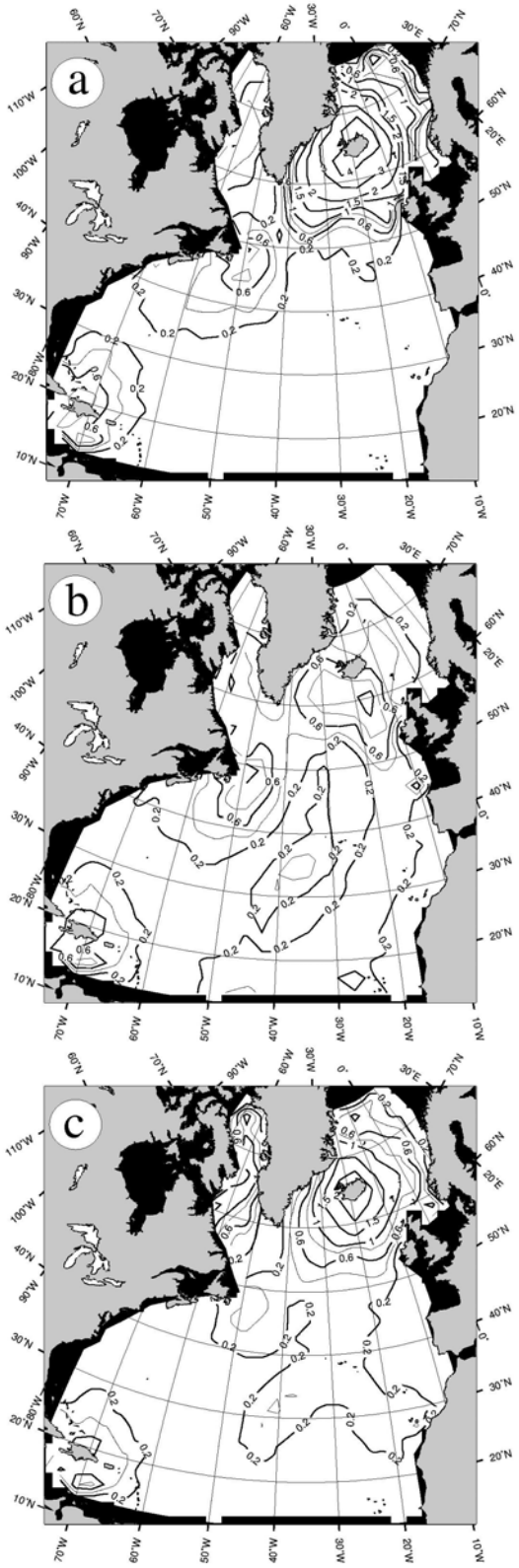

Figure 2. Sedimentation rate (cm/1000 yr.) predicted by sediment transport model using the HM (a), the LGM (b) and the MWE ocean circulation patterns from the OGCM (see text).

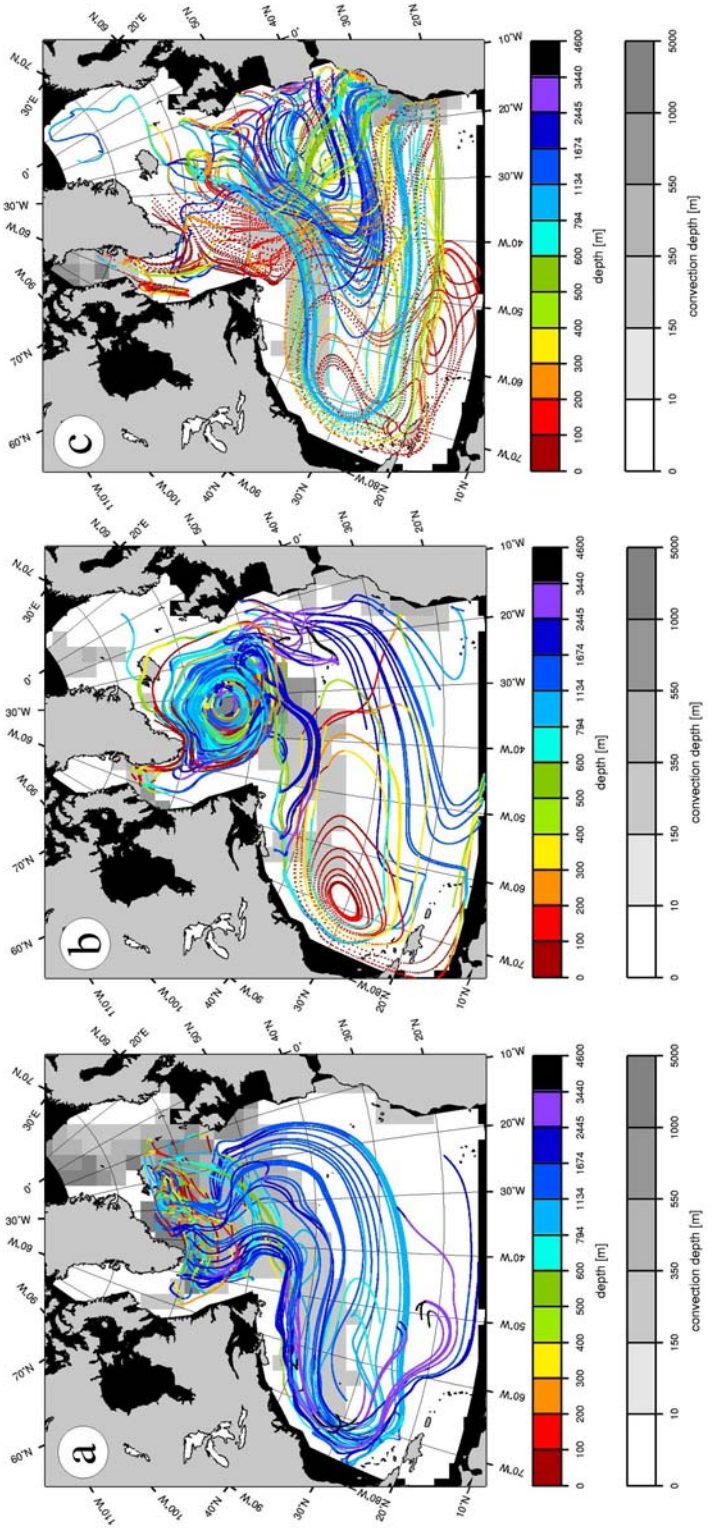

Figure 3. Trajectories of particles deployed at the HM in the central part of the northern North Atlantic: a) Holocene/Modern; b) LGM; c) MWE. The convection depths are shown by different shades of gray. First 100 years of the particles' history are shown. Depth is indicated by colors from the color palette; as the particle descends or upwells the color of the trajectory changes.

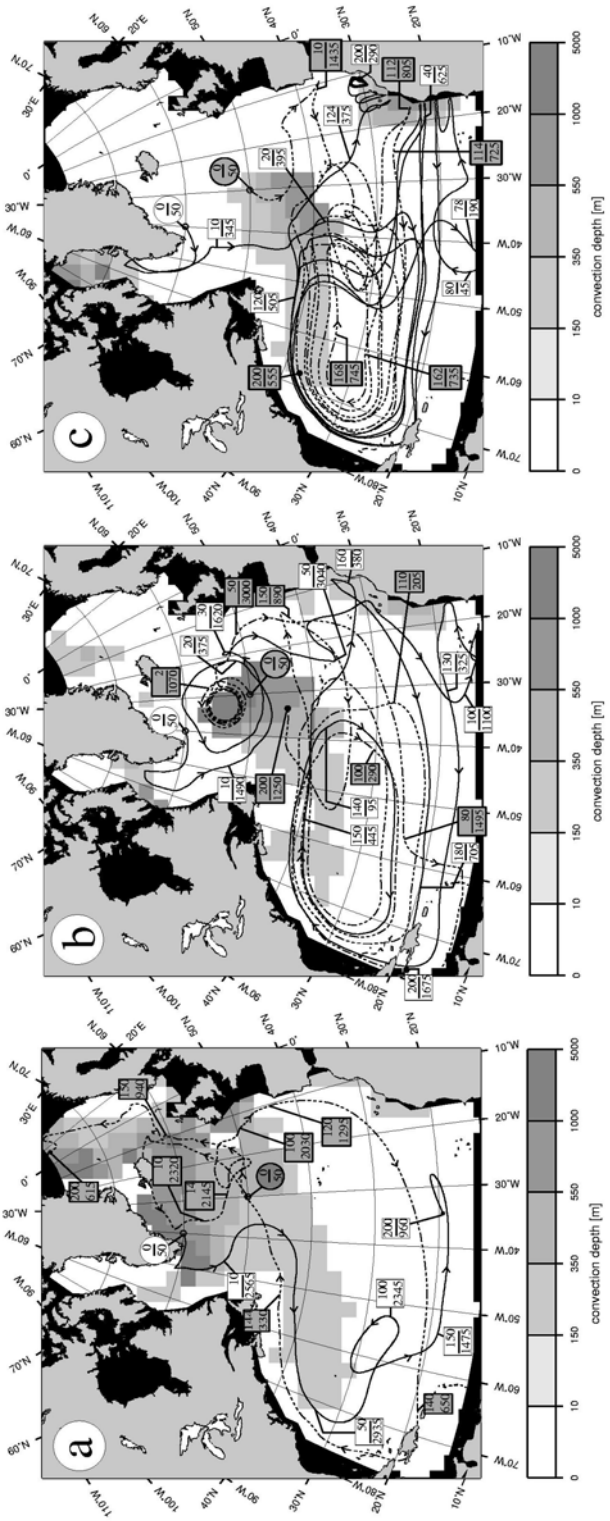

Figure 4. 200–year history of pairs of Lagrangian particles for HM (a), LGM (b), and MWE (c) from the assemblages shown in Figure 3. Small rectangles show elapsed time and depth; small circles indicate starting points, the arrows show the direction of motion, and the bullets indicate the end points of the trajectories. One of the trajectories of each pair is presented by broken line.

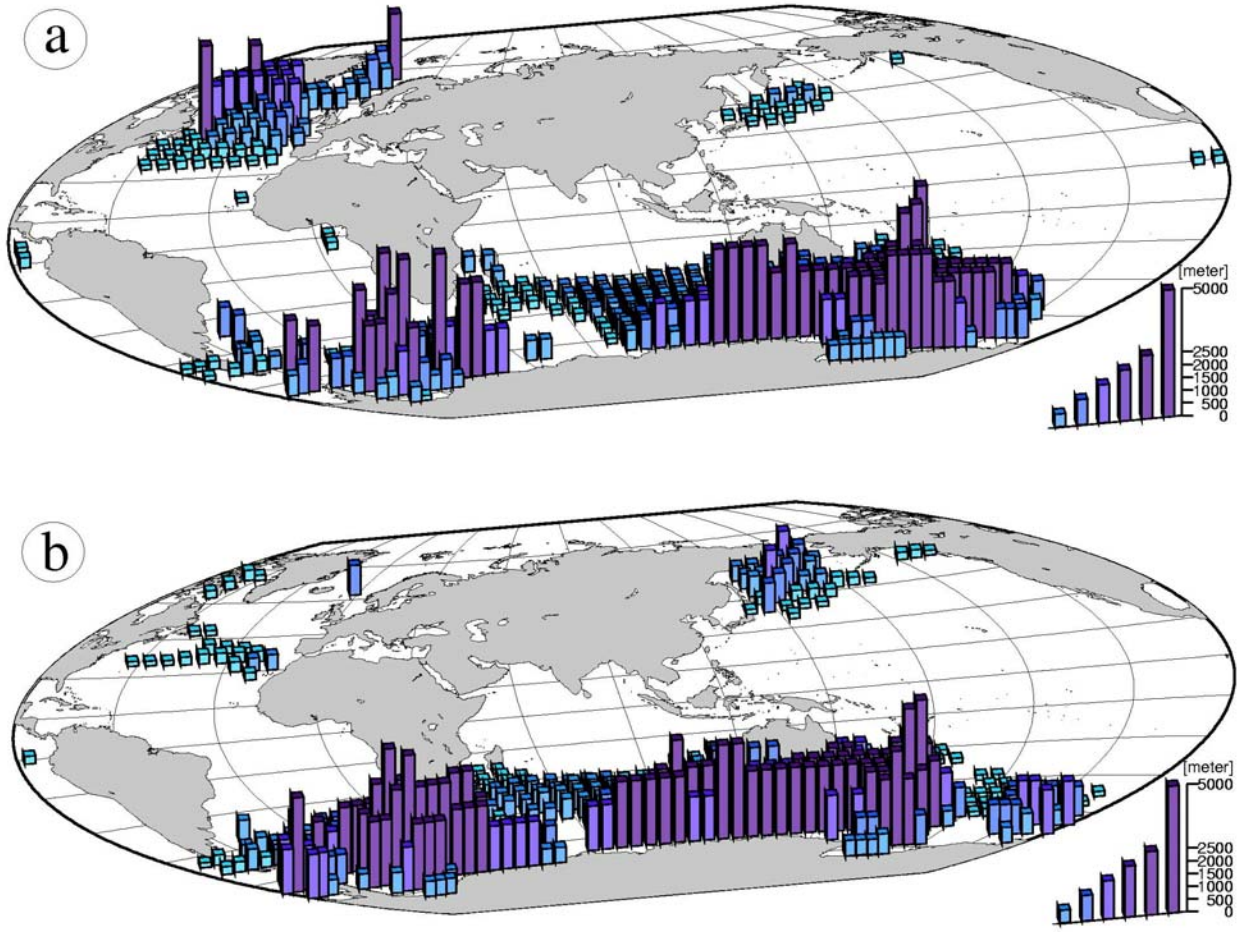

Figure 5. Diagrams of convection: (a) the HM; (b) the LGM. The heights of the bars are equal to the depth of convection.

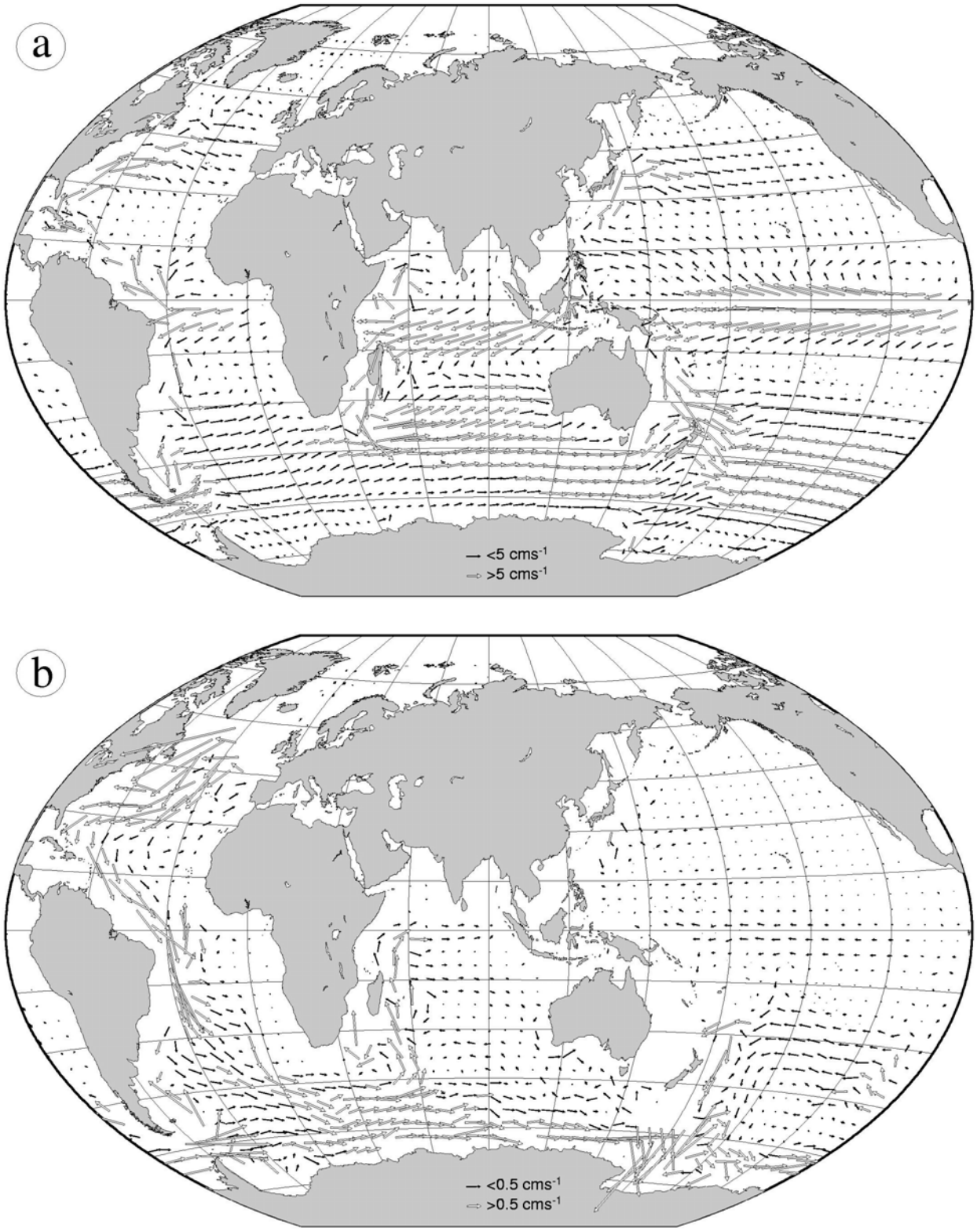

Figure 6. Holocene/Modern velocity vectors at 150 (a) and 2500 m (b). Note different scales for the upper and deep ocean currents.

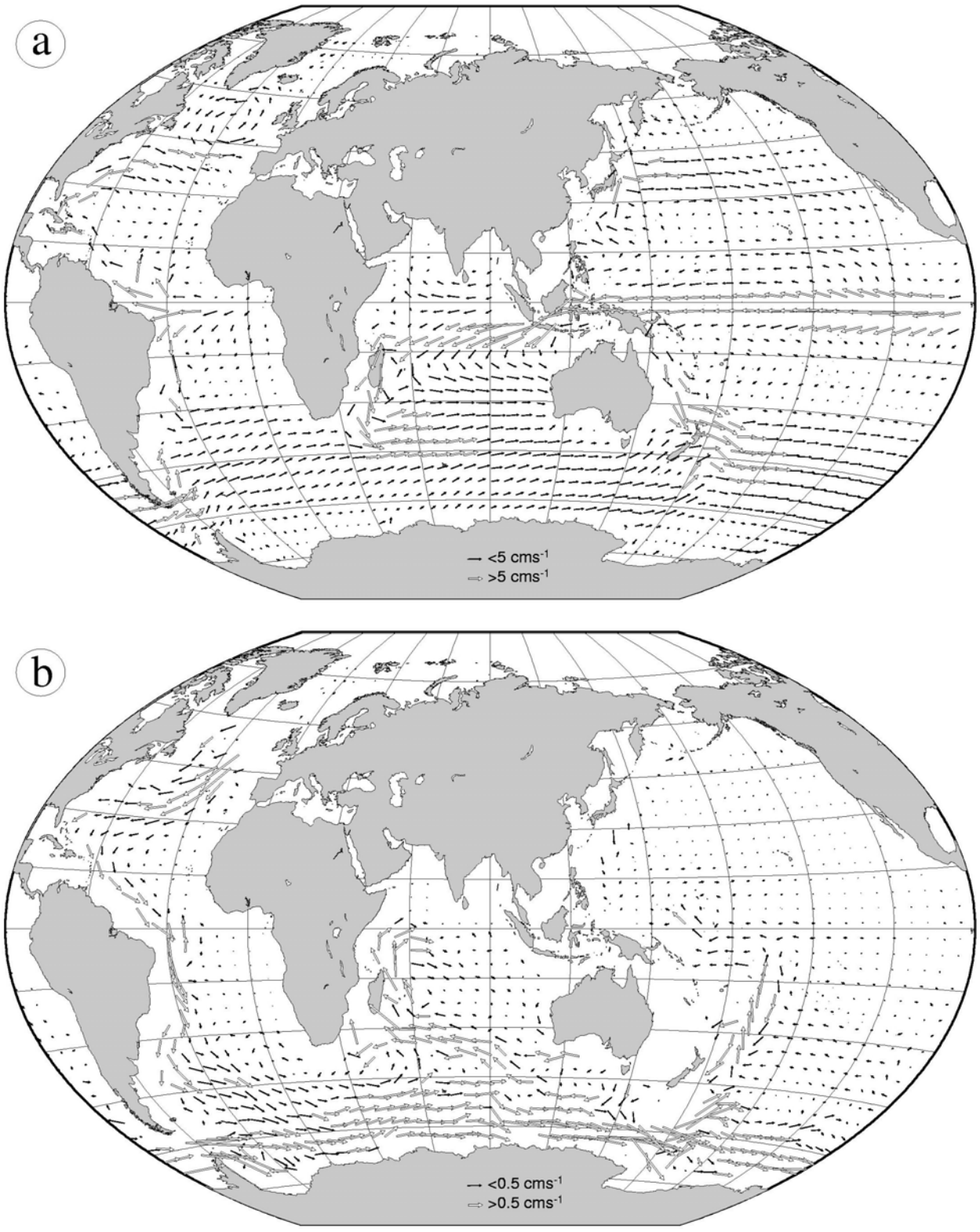

Figure 7. As in Figure 5 for LGM.

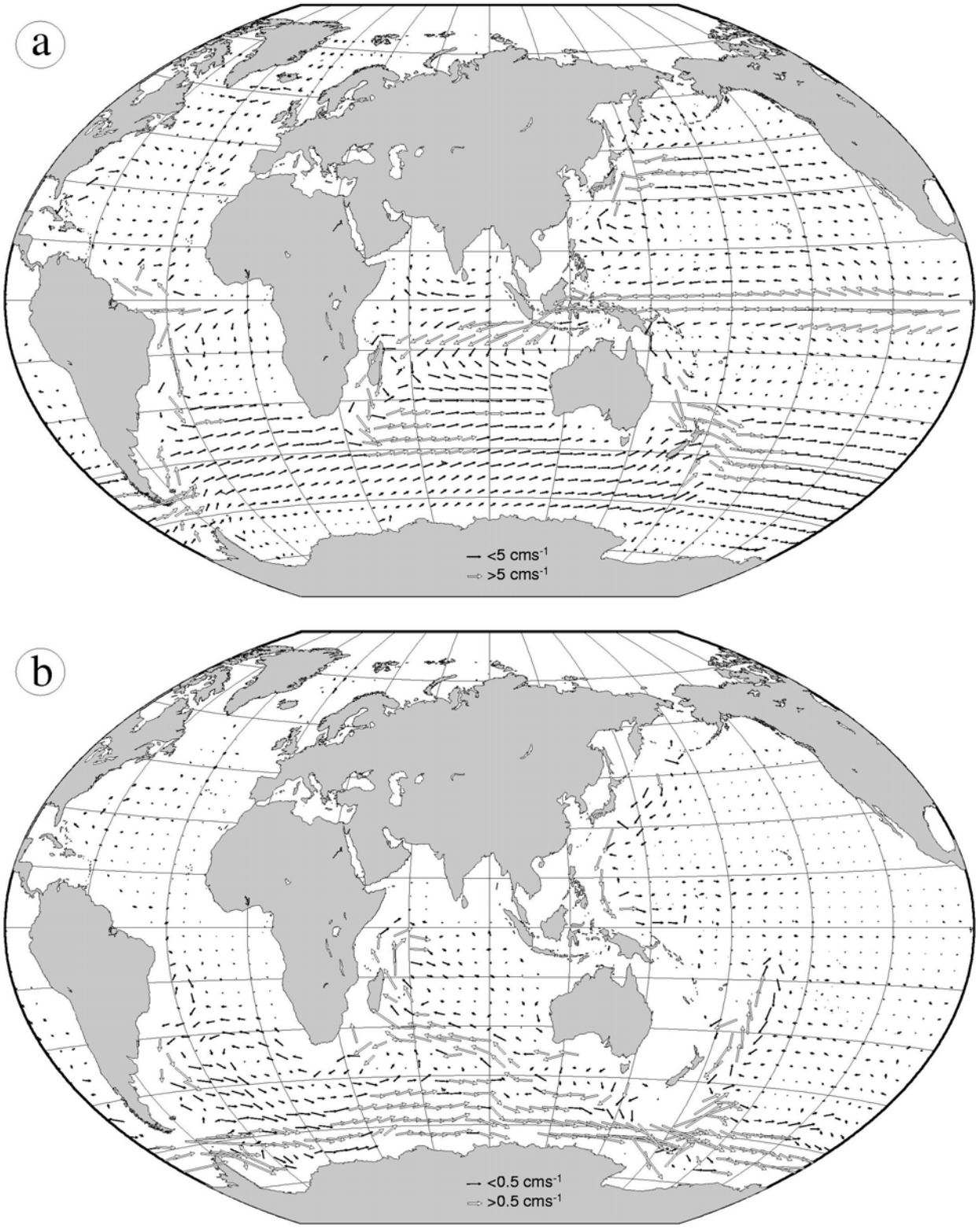

Figure 8. As in Figure 5 for MWE.

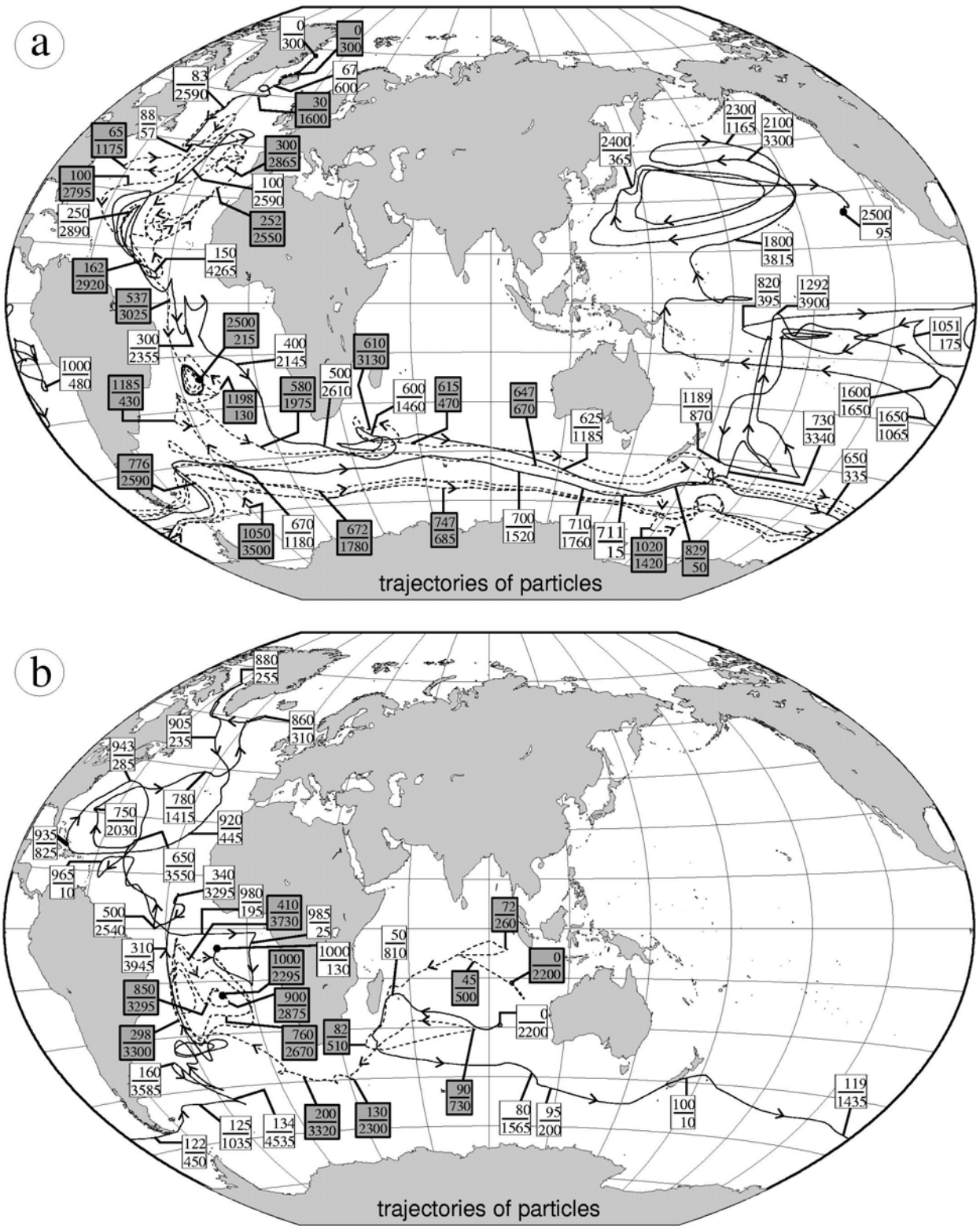

Figure 9. Pairs of trajectories (one trajectory is shown as a solid and the other as a dashed line) visualizing the deep ocean conveyor: a) modern conveyor; b) MWE. Small rectangles show time elapsed after deployment (upper numbers) and the depth at which the particle is found on the trajectory at that time (see Figure 4).